identify the genes involved in the biosynthesis of specific glycans because, as the glycan-biosynthesis enzymes are responsible for producing the glycan ligands, this information will help elucidate the regulation of biological events mediated by glycan-binding proteins.

Systematic methodological merit of CIRES

The experimental setup for CIRES is relatively simple. Briefly, we first made a cross-sample comparison of glycan-related gene expression profiles using cDNA microarrays. This technique yielded the relative expression level for each gene as compared with a universal reference RNA, producing an expression profile for each gene. We then used anti-glycan lectin probes to obtain binding profiles in the same cell lines and compared the two types of profiles. We used the same cross-sample profiles of glycan-related gene expression for the correlation analyses of all the lectins examined in this study.

The cells that we used for gene expression profiling are available either commercially or from a non-profit cell resource center (Japanese Collection of Research Bioresources; JCRB). All cells were cultured under commonly used conditions and were used in logarithmic growth phase. Under these conditions, the glycan expression phenotype obtained by lectin staining tended to be uniform within a cell line and unique for each cell line. Thus, the data obtained by lectin staining with excess probe were suitable for determining the mean fluorescence intensity (MFI) of lectin staining.

This method compared the relative glycan expression profiles of cell lines whose cellular size and character might not be uniform; therefore, we normalized the staining signal by using the ratio of the stained sample MFI to the control MFI. This eliminates the absolute glycan expression signals and normalizes the relative expression results to the staining and data acquisition conditions.

The statistical analysis is the core of the CIRES method. Since glycosylation follows a defined pathway, we could have set up an algorithm suitable for the correlation analyses. However, we chose to use the well-established Pearson's correlation coefficient for the analyses. Regardless of the calculation method, correlations were detected even when the profiles did not completely match. Based on these calculations, a list of genes can be ordered according to the strength of their correlation. This list might be useful in designing further experiments to confirm biological functions.

In glycan biosynthesis, not all relationships are positive in nature, and some lectins used in this study yielded negative correlations. Thus, it is possible to detect dominant inhibitors of specific glycan biosynthesis steps using CIRES. Moreover, in theory, CIRES is not limited to glycan biosynthesis but could be used in any system for which numeric phenotypic expression results (such as glycan expression) can be obtained for a set of cultured cells. The correlation of non-glycosylation phenotypes with gene expression in the same system should be possible.

Systematic methodology for using microarray data in CIRES

One limitation of the standard microarray technique is that it can only detect the relative cDNA expression levels of two samples. This was actually useful when we took the ratio of the signal for each gene relative to that for reference RNA, thus circumventing the microarray problems associated with spot-to-spot variation and hybridization variation for different nucleotide sequences. Almost all of the spots hybridized with universal reference RNA (data not shown). Normal, uniform cell culture conditions were used in this experiment to maximize reproducibility.

In order to calculate the gene expression ratios in a cross-sample manner, we wanted to avoid negative signals in the microarray scans. To do this, we directly used the raw data, instead of applying a cut-off value to the microarray signal by deducting the local background signal from the raw spot signals. We consider this to be a valid option, because we confirmed that the scanner readout after hybridization was reproducible, even for spots yielding weaker signals, and that both options yielded a similar order of relative strength (data not shown).

Normalization was also important because the array results were compared in a cross-sample manner. Sum-based normalization was applied to obtain better correlation coefficients for proven lectins (data not shown). The validity of the calculations was dependent on the use of a consistent standard, making a universal reference essential for the cross-sample comparison. In general, the microarray results tended to be more consistent for stronger hybridization signals than for weaker signals.

Expected and unexpected findings with CIRES

For an epitope whose expression is regulated by a single gene product in its biosynthetic pathway and for which the supply of substrate for that biosynthetic reaction is abundant, CIRES will identify the gene involved in the biosynthesis of the epitope. The finding that the RCA120staining profile did not correlate with a specific glycosyltransferase was therefore not surprising, because it binds LacNAc. Generally, we obtained better correlation coefficients for epitopes created by terminal modifications of LacNAc. CIRES was also useful in identifying major genes responsible for epitope capping, which is negatively correlated with glycan expression, as in the case of PNA.

Our CIRES results tended to show correlations with the GlcNAc transferases. This may result from the use of flow cytometry to detect lectin binding, and thus glycan expression, because lectin staining preferentially detects glycans that extend beyond the glycocalyx. Moreover, the level of epitope expression may not linearly correlate with the lectin signal, because lectins tend to form multimers. As poly-LacNAcs are the usual core units for the presentation of some functional glycan epitopes, GlcNAc transferases found to correlate could also be important for the epitope presentation suitable for lectin-based recognition.

Thus far, we have not identified any enzymes other than glycosyltransferases that strongly correlate with epitope expression levels. However, a subtle negative correlation was noted between the expression of the Con-A epitope and mannosidase expression. Our failure to identify additional enzymes might have resulted from the limited number of lectins available to us. In theory, other factors involved in biosynthetic pathways, such as factors involved in sugar-nucleotide biosynthesis or transport, could also regulate glycan expression on the cell surface.

Limitations of CIRES

Specific probes are unquestionably important for the successful application of CIRES. The most important aspect of lectin specificity is not affinity for the glycan ligand but rather the exclusivity of the enzyme. To calculate statistically significant correlations, a set of cell lines expressing different amounts of the target glycan should be used. The uniform expression of the target glycan in the cell set is undesirable.

To evaluate this methodology, we used the plant lectins that have been used extensively in other glycan studies. Since the correlations are identified by statistical calculations alone, we first assessed those lectins that had already been correlated with specific enzyme genes, to test for the identification of genes that matched glycan expression only by chance. Therefore, when CIRES is applied using uncharacterized glycan-binding probes, the bi-

ological relevance of the correlated genes must be confirmed by altering their expression in the cells. This requirement could be viewed as a limitation of the system. However, the alteration of target glycan expression has been an enduring and major objective of glycobiological experiments concerning lectins. As indicated in Figure 1, the CIRES methodology includes confirmation of the correlation by using glycan-related gene overexpression or silencing. Confirming biological relevance via the transfer of a correlated gene has the additional benefit of providing cells with a different expression level of the epitope of interest, which can be valuable for further assessment of lectin recognition in biological systems. Changing the cell surface expression of glycans for specific anti-glycan probes has been difficult, because the rate-limiting glycosyltransferase must be identified and overexpressed. Thus, allowing for a glycan-related gene transfer procedure that produces glycan-altered cells for further experiments is a major merit of the CIRES methodology.

CIRES alone cannot identify the specific glycan structure to which an anti-glycan probe binds; at the same time, knowledge of the structure of interest does not necessarily mean that modifying its expression on cells is possible. Using the CIRES method will likely result in the production of cells with modified glycan expression, but the actual structure bound by the probe may be unknown. This situation is somewhat similar to that of glycan-array binding studies, in which the probe that binds best on the glycan array does not necessarily bind the same glycan on the array as on cells and the identification of the glycan structure does not always result in the identification of the relevant biosynthetic enzyme. Thus, CIRES could be combined with conventional glycan-binding assays [44–46] to determine the specificity of glycan binding in a set of glycans and to identify the gene that modulates glycan expression on the cell surface, from among the pathway component enzymes. Thus, CIRES is a highly useful genetic strategy for studying the functionality of the interactions between glycans and glycan-binding proteins in cell-based systems.

MATERIALS AND METHODS

Reagents and cell culture

Two commercially available sets of biotin-conjugated plant lectins (Plant Lectin Set I and II) were obtained from Seikagaku (Tokyo, Japan). R-Phycoerythrin-conjugated streptavidin was obtained from Caltag (USA). The B-cell lines Daudi, Namalwa, Raji, Ramos, KMS-BM, and KMS-PE were obtained from the Japanese Collection of Research Bioresources and were cultured in RPMI 1640 medium supplemented with 10% fetal bovine serum, sodium pyruvate, non-essential amino acids, and 2-mercaptoethanol.

DNA microarrays

Gene expression profiling of the six B-cell lines was performed using a glycan-focused cDNA microarray (RIKEN human glycogene microarray, version 1) and a GEO Platform (GPL #3465) and compared with reference RNA (Clontech, USA) to create GEO Series GSE 4407, as reported elsewhere [11].

Flow cytometry

A total of 2.5×10^5 B cells in 100 μl FACS buffer (1% BSA and NaN_3 in PBS(−)) was incubated with excess biotinylated plant lectin probes at room temperature for 30 min. R-Phycoerythrin- or FITC-conjugated streptavidin was used to detect lectin binding. Data were obtained using FACScan or FACSCaliber (BD Biosciences, USA) and analyzed using FlowJo (Tristar, USA) or Cellquest software (BD Biosciences, USA). To cross-compare staining signals between cell lines, the mean fluorescence intensity (MFI) of the background staining was adjusted to around 10, and the relative staining signal was expressed as the ratio of sample MFI divided by the control MFI.

Statistical analysis

Fluorochrome signals on the microarray were acquired by an array scanner (Affymetrix 428) without background subtraction and were then background-corrected using a smoothing function [47]. They were then Lowess normalized using Linear Models for Microarray Data (LIMMA) [48] and the software program R [49]. Inter-array normalization was not used in cross-sample comparisons, as it seemed to cause over-normalization.

The signal from the B-cell lines was divided by the signal from the universal reference RNA [11] to obtain the relative expression profile for each gene in each cell line (Table S1). The gene expression profiles were compared with the lectin staining profiles obtained by flow cytometry. Similarities between the profiles were evaluated with Pearson's correlation coefficient, and probability values (P) were calculated using the correlation coefficient test. For a sample size of six, a correlation coefficient of 0.81 indicates a statistical significance level of 5%. The genes that correlated with lectin staining by this method were ranked according to correlation strength (Table S2), and this list was examined for genes that appeared to be relevant to previously reported lectin glycan epitopes and glycan biosynthetic pathways (Figure 1).

Retrovirus-mediated transduction of glycan-related genes

Retroviruses were prepared and were used to infect Namalwa cells, as reported previously [11]. Briefly, full-length glycosyltransferase cDNA was cloned into a modified MSCV vector, which expressed cDNA and EGFP via an internal ribosome entry site. The plasmid was transiently transfected into Plat-A packaging cells [50], and retrovirus-containing supernatants were collected. Namalwa cells were spin-infected (2000 rpm, 32°C, 120 min) with the retrovirus in the presence of 6 μg/ml polybrene.

The retrovirus-infected cells were cultured for 2 days after infection before analysis by flow cytometry. EGFP-positive and -negative cells were regarded as infected and non-infected cells, respectively. The staining of these two populations was used as the control.

Lectin blotting

B cells were sonicated in detergent-free lysis buffer [10 mM Tris-HCl (pH 7.6), 1 mM DTT, 1 mM EDTA, 0.25 M sucrose, and protease inhibitor cocktail (Roche)]. Postnuclear supernatants were further ultracentrifuged, and the pellets (membrane fraction) were resuspended in lysis buffer. The suspensions were subjected to lectin blotting with HRP-conjugated PHA-E4. The signal intensity was measured by exposure of the membrane to LAS300 (Fujifilm, Japan).

Sialidase treatment

Sialidase treatment was carried out as reported elsewhere [11]. Briefly, Daudi cells were incubated with sialidase in 100 mM sodium acetate (pH 5.2) at room temperature prior to lectin staining. Sialidases from *Arthrobacter ureafaciens* (AUS; Calbiochem, San Diego, USA) and *Salmonella typhimurium* (Takara, Kusatsu, Japan) were used.

SUPPORTING INFORMATION

Table S1 Complete gene expression profiles obtained from cDNA microarray: Fluorescent Cy3 (universal reference) and Cy5

(each Bcell line) readout data were acquired from the array scanner and following statistical calculations were applied using the software program R. First, background was corrected using "Edward method". Each data was then normalized using Linear Models for Microarray Data (LIMMA) to correct bias between fluorescent dyes. Finally, the Cy5 signal from the B cell lines was divided by the Cy3 signal to obtain the relative expression profile for each spot and resultant relative values were shown in columns I through N for each cells. Column A shows serial number of all spots on microarray and column B through E show physical location of all spots on glass slide-based cDNA microarray.
Found at: doi:10.1371/journal.pone.0001232.s001 (0.31 MB XLS)

Table S2 Lists of correlated genes with lectin staining: This is an Exel file consists of 14 worksheets. First sheet shows full list of genes spotted on the Glycan-focuesed microarray and their gene ID numbers. Following sheets are the lists of genes that exhibited stronger correlation with indicated lectin staining profiles. See "Materials and Methods" for the method applied for calculation.
Found at: doi:10.1371/journal.pone.0001232.s002 (0.40 MB XLS)

ACKNOWLEDGMENTS

The authors thank Dr. Hisashi Narimatsu (AIST) for full-length cDNA clones of glycosyltransferases and Dr. Toshio Kitamura (University of Tokyo) for Plat-A packaging cells. We also thank Drs. Atsushi Kuno (AIST) and Eiji Miyoshi (Osaka University) for helpful discussions about lectin determinants.

Author Contributions

Conceived and designed the experiments: HT YK HY AS YO. Performed the experiments: YN RF HY. Analyzed the data: HT YN RF HY YO GT. Contributed reagents/materials/analysis tools: HT YK AS YO GT. Wrote the paper: HT.

REFERENCES

1. Freeze HH (1999) Monosaccharide Metabolism In: Varki A, Cummings R, Esko JD, Freeze HH, Hart GW, Marth J, eds. Essentials of Glycobiology. New York: Cold Spring Harbor Laboratory Press. pp 69–84.
2. Hirschberg CB, Robbins PW, Abeijon C (1998) Transporters of nucleotide sugars, ATP, and nucleotide sulfate in the endoplasmic reticulum and Golgi apparatus Annu Rev Biochem 67: 49–69 9759482.
3. Kornfeld R, Kornfeld S (1985) Assembly of Asparagine-Linked Oligosaccharides Annu Rev Biochem 54: 631–664.
4. Aruffo A, Seed B (1987) Molecular cloning of a CD28 cDNA by a high-efficiency COS cell expression system Proc Natl Acad Sci U S A 84: 8573–7 2825196.
5. Seed B, Aruffo A (1987) Molecular cloning of the CD2 antigen, the T-cell erythrocyte receptor, by a rapid immunoselection procedure Proc Natl Acad Sci U S A 84: 3365–9 2437578.
6. Larsen RD, Rajan VP, Ruff MM, Kukowska-Latallo J, Cummings RD, et al. (1989) Isolation of a cDNA encoding a murine UDPgalactose:beta-D-galactosyl-1,4-N-acetyl-D-glucosaminide alpha-1,3-galactosyltransferase: expression cloning by gene transfer Proc Natl Acad Sci U S A 86: 8227–31 2510162.
7. Narimatsu H (2004) Construction of a human glycogene library and comprehensive functional analysis Glycoconj J 21: 17–24 15467393.
8. Comelli EM, Head SR, Gilmartin T, Whisenant T, Haslam SM, et al. (2006) A focused microarray approach to functional glycomics: transcriptional regulation of the glycome Glycobiology 16: 117–31 16237199.
9. Takematsu H, Kozutsumi Y (2007) DNA microarray in glycobiology In: Greet-Jan B, Lee YC, Suzuki A, Taniguchi N, Voragen AGJ, eds. Comprehensive Glycoscience vol. 2. Oxford: Elsevier. pp 428–448.
10. Kawano S, Hashimoto K, Miyama T, Goto S, Kanehisa M (2005) Prediction of glycan structures from gene expression data based on glycosyltransferase reactions Bioinformatics 21: 3976–82 16159923.
11. Naito Y, Takematsu H, Koyama S, Miyake S, Yamamoto H, et al. (2007) Germinal center marker GL7 probes activation-dependent repression of N-glycolylneuraminic acid, a sialic acid species involved in the negative modulation of B cell activation Mol Cell Biol 27: 3008–3022.
12. Fernandes B, Sagman U, Auger M, Demetrio M, Dennis JW (1991) Beta 1-6 branched oligosaccharides as a marker of tumor progression in human breast and colon neoplasia Cancer Res 51: 718–23 1985789.
13. Yamamoto H, Swoger J, Greene S, Saito T, Hurh J, et al. (2000) Beta1,6-N-acetylglucosamine-bearing N-glycans in human gliomas: implications for a role in regulating invasivity Cancer Res 60: 134–42 10646865.
14. Granovsky M, Fata J, Pawling J, Muller WJ, Khokha R, et al. (2000) Suppression of tumor growth and metastasis in Mgat5-deficient mice Nat Med 6: 306–12 10700233.
15. Partridge EA, Le Roy C, Di Guglielmo GM, Pawling J, Cheung P, et al. (2004) Regulation of cytokine receptors by Golgi N-glycan processing and endocytosis Science 306: 120–4 15459394.
16. Hennet T, Chui D, Paulson JC, Marth JD (1998) Immune regulation by the ST6Gal sialyltransferase Proc Natl Acad Sci U S A 95: 4504–9 9539767.
17. Kuno A, Uchiyama N, Koseki-Kuno S, Ebe Y, Takashima S, et al. (2005) Evanescent-field fluorescence-assisted lectin microarray: a new strategy for glycan profiling Nat Methods 2: 851–6 16278656.
18. Gillespie W, Paulson JC, Kelm S, Pang M, Baum LG (1993) Regulation of alpha 2,3-sialyltransferase expression correlates with conversion of peanut agglutinin (PNA)+ to PNA- phenotype in developing thymocytes J Biol Chem 268: 3801–4 8440675.
19. Priatel JJ, Chui D, Hiraoka N, Simmons CJ, Richardson KB, et al. (2000) The ST3Gal-I sialyltransferase controls CD8+ T lymphocyte homeostasis by modulating O-glycan biosynthesis Immunity 12: 273–83 10755614.
20. Kaifu R, Osawa T, Jeanloz RW (1975) Synthesis of 2-O-(2-acetamido-2-deoxy-beta-D-glucopyranosyl)-D-mannose, and its interaction with D-mannose-specific lectins Carbohydr Res 40: 111–7 1125946.
21. Shinkawa T, Nakamura K, Yamane N, Shoji-Hosaka E, Kanda Y, et al. (2003) The absence of fucose but not the presence of galactose or bisecting N-acetylglucosamine of human IgG1 complex-type oligosaccharides shows the critical role of enhancing antibody-dependent cellular cytotoxicity J Biol Chem 278: 3466–73 12427744.
22. Wang X, Inoue S, Gu J, Miyoshi E, Noda K, et al. (2005) Dysregulation of TGF-beta1 receptor activation leads to abnormal lung development and emphysema-like phenotype in core fucose-deficient mice Proc Natl Acad Sci U S A 102: 15791–6 16236725.
23. Matsumoto I, Osawa T (1969) Purification and characterization of an anti-H(O) phytohemagglutinin of Ulex europeus Biochim Biophys Acta 194: 180–9 5353123.
24. Okajima T, Fukumoto S, Miyazaki H, Ishida H, Kiso M, et al. (1999) Molecular cloning of a novel alpha2,3-sialyltransferase (ST3Gal VI) that sialylates type II lactosamine structures on glycoproteins and glycolipids J Biol Chem 274: 11479–86 10206952.
25. Ito N, Imai S, Haga S, Nagaike C, Morimura Y, et al. (1996) Localization of binding sites of Ulex europaeus I, Helix pomatia and Griffonia simplicifolia I-B4 lectins and analysis of their backbone structures by several glycosidases and poly-N-acetyllactosamine-specific lectins in human breast carcinomas Histochem Cell Biol 106: 331–9 8897074.
26. Furukawa K, Sato T (1999) Beta-1,4-galactosylation of N-glycans is a complex process Biochim Biophys Acta 1473: 54–66 10580129.
27. Crowley JF, Goldstein IJ, Arnarp J, Lonngren J (1984) Carbohydrate binding studies on the lectin from Datura stramonium seeds Arch Biochem Biophys 231: 524–33 6203486.
28. Yamashita K, Totani K, Ohkura T, Takasaki S, Goldstein IJ, et al. (1987) Carbohydrate binding properties of complex-type oligosaccharides on immobilized Datura stramonium lectin J Biol Chem 262: 1602–7 3805046.
29. Ihara Y, Nishikawa A, Taniguchi N (1995) Effects of dibutyryl cAMP and bromodeoxyuridine on expression of N-acetylglucosaminyltransferases III and V in GOTO neuroblastoma cells Glycoconj J 12: 787–94 8748156.
30. Sasai K, Ikeda Y, Eguchi H, Tsuda T, Honke K, et al. (2002) The action of N-acetylglucosaminyltransferase-V is prevented by the bisecting GlcNAc residue at the catalytic step FEBS Lett 522: 151–5 12095636.
31. Miyoshi E, Nishikawa A, Ihara Y, Hayashi N, Fusamoto H, et al. (1994) Selective suppression of N-acetylglucosaminyltransferase III activity in a human hepatoblastoma cell line transfected with hepatitis B virus Cancer Res 54: 1854–8 8137300.
32. Sultan AS, Miyoshi E, Ihara Y, Nishikawa A, Tsukada Y, et al. (1997) Bisecting GlcNAc structures act as negative sorting signals for cell surface glycoproteins in forskolin-treated rat hepatoma cells J Biol Chem 272: 2866–72 9006930.
33. Wang WC, Cummings RD (1988) The immobilized leukoagglutinin from the seeds of Maackia amurensis binds with high affinity to complex-type Asn-linked oligosaccharides containing terminal sialic acid-linked alpha-2,3 to penultimate galactose residues J Biol Chem 263: 4576–85 3350806.
34. Konami Y, Yamamoto K, Osawa T, Irimura T (1994) Strong affinity of Maackia amurensis hemagglutinin (MAH) for sialic acid-containing Ser/Thr-linked carbohydrate chains of N-terminal octapeptides from human glycophorin A FEBS Lett 342: 334–8 8150094.
35. Knibbs RN, Goldstein IJ, Ratcliffe RM, Shibuya N (1991) Characterization of the carbohydrate binding specificity of the leukoagglutinating lectin from Maackia amurensis. Comparison with other sialic acid-specific lectins J Biol Chem 266: 83–8 1985926.

36. Stanley P, Caillibot V, Siminovitch L (1975) Selection and characterization of eight phenotypically distinct lines of lectin-resistant Chinese hamster ovary cell Cell 6: 121–8 1182798.
37. Kitagawa H, Paulson JC (1994) Differential expression of five sialyltransferase genes in human tissues J Biol Chem 269: 17872–8 8027041.
38. Bierhuizen MF, Mattei MG, Fukuda M (1993) Expression of the developmental I antigen by a cloned human cDNA encoding a member of a beta-1,6-N-acetylglucosaminyltransferase gene family Genes Dev 7: 468–78 8449405.
39. Moremen KW (2002) Golgi alpha-mannosidase II deficiency in vertebrate systems: implications for asparagine-linked oligosaccharide processing in mammals Biochim Biophys Acta 1573: 225–35 12417404.
40. Chen Y, Jain RK, Chandrasekaran EV, Matta KL (1995) Use of sialylated or sulfated derivatives and acrylamide copolymers of Gal beta 1,3GalNAc alpha- and GalNAc alpha- to determine the specificities of blood group T- and Tn-specific lectins and the copolymers to measure anti-T and anti-Tn antibody levels in cancer patients Glycoconj J 12: 55–62 7795413.
41. Nakamura-Tsuruta S, Kominami J, Kuno A, Hirabayashi J (2006) Evidence that Agaricus bisporus agglutinin (ABA) has dual sugar-binding specificity Biochem Biophys Res Commun 347: 215–20 16824489.
42. Hakomori S (2004) Carbohydrate-to-carbohydrate interaction in basic cell biology: a brief overview Arch Biochem Biophys 426: 173–81 15158668.
43. Paulson JC, Blixt O, Collins BE (2006) Sweet spots in functional glycomics Nat Chem Biol 2: 238–48 16619023.
44. Fukui S, Feizi T, Galustian C, Lawson AM, Chai W (2002) Oligosaccharide microarrays for high-throughput detection and specificity assignments of carbohydrate-protein interactions Nat Biotechnol 20: 1011–7 12219077.
45. Blixt O, Head S, Mondala T, Scanlan C, Huflejt ME, et al. (2004) Printed covalent glycan array for ligand profiling of diverse glycan binding proteins Proc Natl Acad Sci U S A 101: 17033–8 15563589.
46. Kamekawa N, Hayama K, Nakamura-Tsuruta S, Kuno A, Hirabayashi J (2006) A combined strategy for glycan profiling: a model study with pyridylaminated oligosaccharides J Biochem (Tokyo) 140: 337–47 16861248.
47. Edwards D (2003) Non-linear normalization and background correction in one-channel cDNA microarray studies Bioinformatics 19: 825–33 12724292.
48. Smyth GK (2005) Limma: linear models for microarray data. In: R. Gentleman VC, S. Dudoit, R. Irizarry, W. Huber, eds. 'Bioinformatics and Computational Biology Solutions using R and Bioconductor'. New York: Springer. pp Chapter 23.
49. Team RDC (2004) R: A Language and Environment for Statistical Computing. Vienna: R Foundation for Statistical Computing, http://www.R-project.org.
50. Morita S, Kojima T, Kitamura T (2000) Plat-E: An efficient and stable system for transient packaging of retroviruses Gene Ther 7: 1063–6 10871756.
51. Cummings R (1999) Plant Lectins. In: Varki A, Cummings R, Esko JD, Freeze HH, Hart GW, Marth J. Essentials of Glycobiology. New York: Cold Spring Harbor Laboratory Press. pp 455–468.

Available online at www.sciencedirect.com
ScienceDirect
ELSEVIER
Biochemical and Biophysical Research Communications 363 (2007) 835–839
BBRC
www.elsevier.com/locate/ybbrc

Abnormal features in mutant cerebellar Purkinje cells lacking junctophilins

Atsushi Ikeda [a,1], Taisuke Miyazaki [b,1], Sho Kakizawa [c], Yasushi Okuno [d], Soken Tsuchiya [d], Akira Myomoto [d], Shin-ya Saito [e], Tetsuji Yamamoto [a], Tetsuo Yamazaki [a], Masamitsu Iino [c], Gozoh Tsujimoto [d], Masahiko Watanabe [b], Hiroshi Takeshima [a,e,*]

[a] *Department of Biological Chemistry, Graduate School of Pharmaceutical Sciences, Kyoto University, Kyoto 606-8501, Japan*
[b] *Department of Anatomy, Hokkaido University Graduate School of Medicine, Sapporo, Japan*
[c] *Department of Pharmacology, Graduate School of Medicine, The University of Tokyo, Tokyo, Japan*
[d] *Department of Genomic Drug Discovery Science, Graduate School of Pharmaceutical Sciences, Kyoto University, Kyoto 606-8501, Japan*
[e] *Department of Medical Chemistry, Tohoku University Graduate School of Medicine, Sendai, Japan*

Received 1 September 2007
Available online 24 September 2007

Abstract

Junctional membrane complexes (JMCs) generated by junctophilins are required for Ca^{2+}-mediated communication between cell-surface and intracellular channels in excitable cells. Knockout mice lacking neural junctophilins (JP-DKO) show severe motor defects and irregular cerebellar plasticity due to abolished channel crosstalk in Purkinje cells (PCs). To precisely understand aberrations in JP-DKO mice, we further analyzed the mutant PCs. During the induction of cerebellar plasticity via electrical stimuli, JP-DKO PCs showed insufficient depolarizing responses. Immunochemistry detected mild impairment in synaptic maturation and hyperphosphorylation of protein kinase Cγ in JP-DKO PCs. Moreover, gene expression was slightly altered in the JP-DKO cerebellum. Therefore, the mutant PCs bear marginal but widespread abnormalities, all of which likely cause cerebellar motor defects in JP-DKO mice.

Keywords: Long-term depression; Multiple innervation; Protein kinase C; Ryanodine receptor

Functional communications between cell-surface and intracellular channels play indispensable roles in excitable cells [1]. Ca^{2+}-mediated channel crosstalk often takes place in specific subcellular structures, called the junctional membrane complexes (JMCs), which are characterized by close apposition of the endoplasmic/sarcoplasmic reticulum (ER/SR) and the cell membrane [2]. Of four junctophilin (JP) subtypes, JP1 and JP2 contribute to the formation of JMCs in striated muscle [3–5], while JP3 and JP4 are co-expressed in neuron [6]. Double-knockout mice deficient for both neural JPs (JP-DKO) exhibit impaired motor coordination and learning [7]. In cerebellar Purkinje cells (PCs), the generation of slow afterhyperpolarization (sAHP) following the climbing fiber (CF)-mediated complex spike requires Ca^{2+}-mediated channel crosstalk between P/Q-type voltage-gated Ca^{2+} channels (P/Q channels), ryanodine receptor channels (RyRs) and small-conductance Ca^{2+}-activated K^+ channels (SK channels). This channel communication probably occurs in JP-mediated JMCs and is indispensable for long-term depression (LTD) at parallel fiber (PF)-PC synapses. Indeed, this channel crosstalk is severely impaired and an LTD-inducing paradigm adversely leads to long-term potentiation

* Corresponding author. Address: Department of Biological Chemistry, Graduate School of Pharmaceutical Sciences, Kyoto University, Kyoto 606-8501, Japan. Fax: +81 75 753 4605.
E-mail address: takeshim@pharm.kyoto-u.ac.jp (H. Takeshima).
[1] These authors contributed equally to this work.

0006-291X/$ - see front matter © 2007 Elsevier Inc. All rights reserved.
doi:10.1016/j.bbrc.2007.09.062

(LTP) in JP-DKO PCs [7]. In our continuing attempt to deepen understanding of impaired cerebellar functions in JP-DKO mice, we report irregular PC excitability, atypical CF-wiring to PCs, hyperphosphorylation of protein kinase C (PKC) and altered gene expression.

Materials and methods

Electrophysiological measurements. JP-3(−/−) JP-4(−/−) mice (JP-DKO) and JP-3(+/−) JP-4(+/−) mice (JP-DHE) were described previously [8]. For electrophysiological measurements, cerebellar slices were prepared from mice aged 8–10 weeks and whole-cell recordings were performed from PCs [7,9]. LTD was induced by conjunctive stimulation (CJS, 300 single PF stimuli in conjunction with single CF stimuli repeated at 1 Hz for 5 min) after the initial baseline recording for at least 10 min.

Morphological analysis. Morphological analyses were carried out using mice aged 6–10 weeks [10,11]. For anterograde labeling of CFs, the inferior olive in the anesthetized mice were injected with dextran Texas red. After 4 days of survival, mice were fixed by transcardial perfusion, and prepared microslicer sections were immunostained for calbindin and vesicular glutamate transporter type 2 (VGluT2) and analyzed using a confocal microscope.

Microarray, real-time PCR and immunoblot analyses. Total RNA was isolated from the cerebella of male mice aged 6–8 weeks using the Isogen reagent (Nippongene, Japan), fluorescence labeled and hybridized onto the Mouse Genome 430 2.0 Array (Affymetrix). Raw data obtained were analyzed as described previously [12]. Real-time PCR was performed using the Chromo 4 system (Bio-Rad). Cerebellar homogenates were examined by immunoblotting [10] using the following antibodies: total and phosphorylated (p) PKCγ, PDE (phosphodiesterase) 1C (Abcam), pPKCα, pMARCKS (myristoylated alanine-rich C kinase substrate), pNR1 (N-methyl-D-aspartate receptor 1), pGluR1 (glutamate receptor 1), pCREB (cAMP response element-binding protein), pDARPP (Dopamine- and cAMP-regulated neuronal phosphoprotein), Nab2 (Ngfi-A binding protein 2) (Millipore), pERK1/2 (extracellular signal-regulated kinase 1/2), Egr1 (early growth response 1) (Cell Signaling), β-tubulin (Sigma), and pCaMKII (Ca^{2+}/calmodulin-dependent protein kinase II, gift from Dr. Fukunaga, Tohoku University, Japan).

Results and discussion

Atypical depolarizing responses in JP-DKO PCs

In cerebellar slice preparations, CJS to both PF and CF induces LTD at PF-PC synapses [13]. In control mice, PF-evoked excitatory postsynaptic currents (PF-EPSCs) recorded in voltage-clamped PCs were remarkably decreased from the baseline level after CJS. As shown in Fig. 1A and B, this LTD-inducing paradigm adversely led to LTP in JP-DKO slices and control slices treated with apamin, an SK channel inhibitor. It has been reported that PF-LTP is induced by CJS when LTD was previously established at the CF-PC synapse [14] and also that both CF-evoked spikelets and dendritic Ca^{2+} transients are weakened in PCs after the induction of CF-LTD [15]. Based on these findings, we focused on CF-evoked spikelets in JP-DKO PCs. During CJS composed of stimuli repeated 300 times, control PCs showed constant voltage responses of spikelets, whereas spikelet numbers were significantly decreased at the late phase in both JP-DKO and apamin-treated control PCs (Fig. 1C and D). Therefore, the reverse plasticity in JP-DKO and the apamin-treated PCs may be cardinally induced by the impaired spikelets due to insufficient SK channel opening.

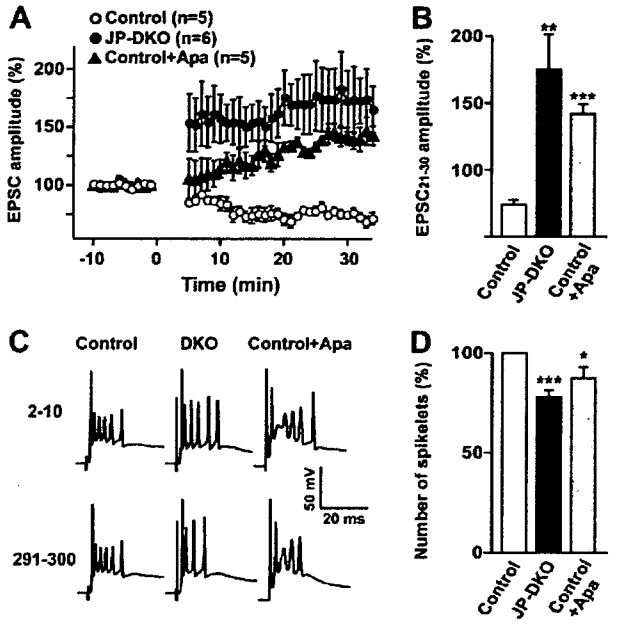

Fig. 1. Deformed spikelets during CJS in JP-DKO and apamin-treated control PCs. (A) PF-EPSCs were normalized by the mean value observed before CJS. Apamin (Apa; 200 nM) was applied to the bathing solution during recording. (B) Average EPSP amplitude during the 21–30 min period after CJS. (C) Representative voltage responses of PCs at early (2–10) and late (291–300) phases during CJS. (D) Averaged spikelet numbers at 291–300th responses normalized by values at 2–10th responses. Data are presented as means ± SEM ($^{*}p < 0.05$, $^{**}p < 0.01$ and $^{***}p < 0.001$ in *t*-test).

In PCs, P/Q channels, rather than voltage-gated Na^{+} channels, predominantly contribute to the generation of the slow spikelets [16]. JP-mediated channel crosstalk between P/Q channels, RyRs, and SK channels generates sAHP following spikelets [7]. Voltage-gated channels incorporate voltage-dependent inactivation features and their recovery from inactivated states requires the repolarization of the membrane potential. As a predicted mechanism underlying the reverse plasticity, sAHP deficiency may prevent the recovery of P/Q channels from the inactivated state and likely weakens spikelets during CJS in both JP-DKO and the apamin-treated PCs. JP-DKO and the apamin-treated PCs showed slight differences in the temporal profile of PF-EPSC potentiation (Fig. 1A). In particular, obvious differences observed immediately after CJS may imply as-yet-unrecognized defects in JP-DKO PCs besides sAHP deficiency due to SK channel dysfunctioning.

Mild disturbance in CF innervation to JP-DKO PCs

In our previous report, PF-PC synapses appeared normal in JP-DKO mice. To morphologically analyze the physical connection between CFs and PCs, CFs were anterogradely labeled (aCF) with dextran Texas red; CF-PC synapses and PC dendrites were visualized with antibodies

against VGluT2 and calbindin, respectively. In control mice (Fig. 2A), aCF precisely followed the branching of PC shaft dendrites and the terminal swellings of aCF overlapped completely with VGluT2. The DKO cerebellum showed no gross morphological abnormalities; PC dendrites were well branched and associated with CF terminals in regular spacing (Fig. 2B1). However, when carefully observed at higher magnifications, the same dendritic shaft innervated by aCF terminals (red arrows) was associated with a few synaptic terminals of tracer-unlabeled CFs (uCF, green arrows) (Fig. 2B2–5). This mild type of multiple CF innervation was often observed in the DKO cerebellum by this anatomical analysis, but was under the detection threshold by electrophysiological analysis [7].

In recent studies, a close correlation between multiple CF innervation and motor discoordination was repeatedly appreciated in a number of knockout mice including mutant mice defective in P/Q channels [11] and PKCγ [17]. Thus, the mild multiple innervation, together with the deranged Ca^{2+}-mediated channel crosstalk [7], may lead to severe motor discoordination in JP-DKO mice. The predominant distribution of JPs to the somatodendritic regions of PCs [6] suggests that PCs, rather than CFs, are likely responsible for the retention of the aberrant CF-PC innervation in adult JP-DKO mice. Because both P/Q channels and PKCγ in PCs are essential for eliminating excess CF-PC synapses, two possibilities are reasonably proposed behind the mild symptom in JP-DKO PCs, i.e., the reduction of P/Q channel-mediated Ca^{2+} influx during repeated depolarization and the predicted hyperactivation of PKCγ (see below).

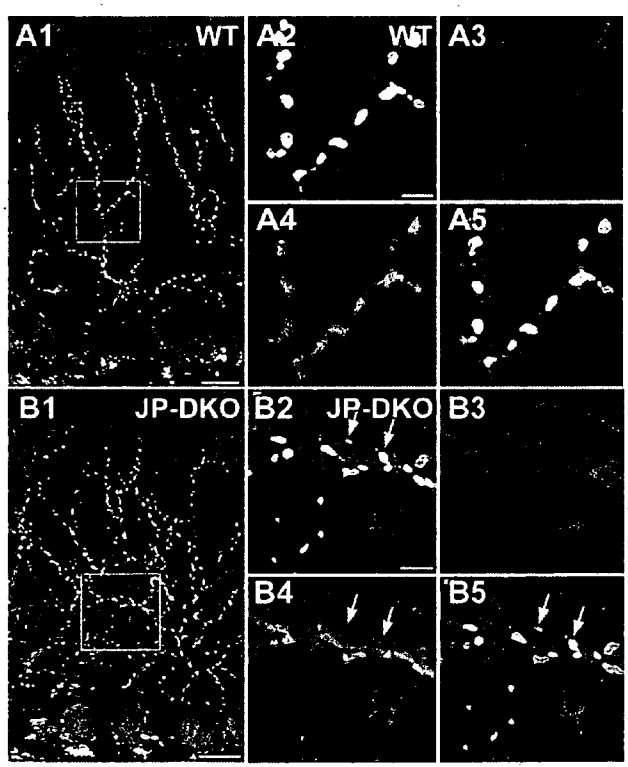

Fig. 2. Aberrant CF-PC innervation in JP-DKO cerebellum. Cerebellar sections were labeled for calbindin (blue), VGluT2 (green) and the anterograde CF tracer dextran Texas red (red) in control (A) and JP-DKO mice (B). Boxed regions in A1 and B1 are magnified in A2–5 and B2–5, respectively. The arrows indicate terminals of anterogradely-labeled CFs (aCF, red arrows) and unlabeled CFs (uCF, green arrows), respectively. Scale bars, 20 μm in A1 and B1; 5 μm in A2–5 and B2–5.

Hyperphosphorylation of PKCγ in JP-DKO PCs

Ca^{2+}-dependent signaling plays a central role for inducing synaptic plasticity such as cerebellar LTD and hippocampal LTP [13]. In our immunoblot analysis, the JP-DKO cerebellum showed an enhanced phosphorylation level at T674 of PKCγ without affecting other phosphorylation sites or its protein content (Fig. 3 and Suppl. Fig. 1). In addition, we did not detect any abnormalities in phosphorylation of well-known PKC substrates (MARCKS and NR1) or of other protein kinases. Since PKCγ is predominantly expressed in PCs among cerebellar cell types, the hyperphosphorylation seems to occur in JP-DKO PCs. Although we have observed regular CF-mediated Ca^{2+} responses in JP-DKO PC soma regions [7], sAHP deficiency could slightly prolong opening of P/Q channels upon sporadic stimuli. It might be that enhanced Ca^{2+} signaling at the microdomain level stimulates the autophosphorylation of PKCγ in JP-DKO PCs under basal conditions. In addition to facilitated autophosphorylation, PKCγ activation accompanies its translocation to the cell membrane from the cytoplasm. PKCγ was clearly detected in the cytoplasm and on the cell membrane, and no difference was observed in its subcellular localization between control and JP-DKO PCs (Suppl. Fig. 2). Although MARCKS and NR1 showed normal phosphorylation levels, it is still possible that PKCγ activity was enhanced to change phosphorylation states of unknown signaling molecules regulating cerebellar motor functions in JP-DKO PCs. On the other hand, PKCγ-knockout mice suffering severe multiple innervation have established its essential

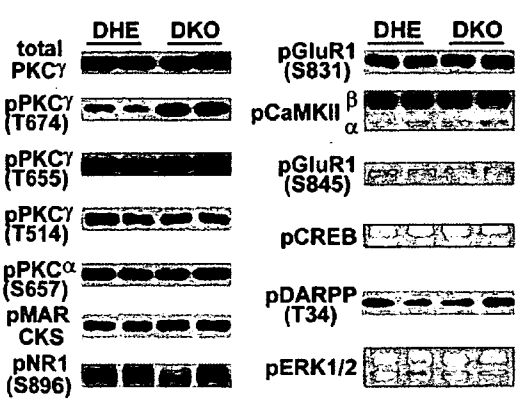

Fig. 3. Hyperphosphorylation at T674 of PKCγ in JP-DKO cerebellum. Representative immunoblot data are shown. The immunoreactivities were statistically analyzed in Suppl. Fig. 1.

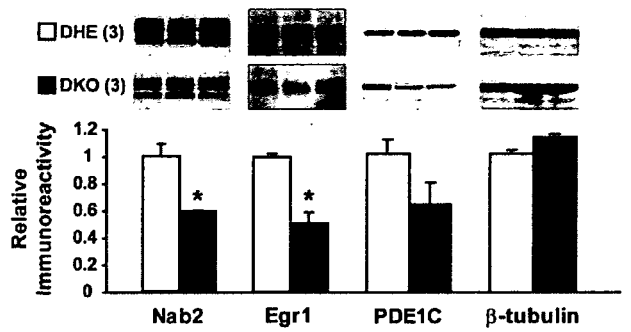

Fig. 4. Reduced expression of Nab2 and Egr1 in JP-DKO cerebellum. Immunoreactivities (upper images) were statistically analyzed. Data are presented as means ± SEM (n values in parentheses, $^*p < 0.05$ in t-test).

role in CF-PC synaptic maturation [17]. Hyperphosphorylated PKCγ might also affect signaling processes for CF elimination in JP-DKO PCs.

Altered gene expression in JP-DKO cerebellum

We finally surveyed altered gene expression in the JP-DKO cerebellum. Our microarray analysis suggested minimally altered gene expression between genotypes (Suppl. Fig. 3), but identified eight up-regulated and three down-regulated candidate genes in JP-DKO mice (Suppl. Table 1). Of the candidates, the down-regulation of *Nab2* was confirmed by real-time PCR and immunoblotting (Fig. 4 and Suppl. Fig. 4). Nab2 is a transcriptional corepressor induced by the zinc-finger transcription factor Egr1, which is up-regulated by neuronal stimuli and essential for LTP in hippocampal neurons [18]. In the JP-DKO cerebellum, Egr1 protein was obviously decreased (Fig. 4). The reduced Nab2 and Egr1 levels may be due to less electrically-active properties in JP-DKO PCs exhibiting the impaired spikelets (Fig. 1).

Although we need to examine the precise linkage between JP deficiency and several abnormalities reported here, they may be directly or indirectly connected with sAHP deficiency in JP-DKO PCs as discussed above. These chronic abnormalities observed under normal housing conditions likely further aggravate weakened spikelets caused by the sAHP deficiency to produce the severity of the reverse plasticity in the JP-DKO cerebellum. Our previous study suggests impairments of overall brain functions, including the salivary reflex and hippocampus-dependent memory in JP-DKO mice [8]. The presented data clearly suggest that JP-mediated JMCs are essential for a broad range of cellular homeostasis in various neurons.

Acknowledgments

This work was supported in part by grants from the Ministry of Education, Culture, Sports, Science, and Technology of Japan, the Naito Foundation, the Sumitomo Foundation, the Uehara Memorial Foundation, the Life Science Foundation, and the Takeda Science Foundation.

Appendix A. Supplementary data

Supplementary data associated with this article can be found, in the online version, at doi:10.1016/j.bbrc.2007.09.062.

References

[1] M.J. Berridge, M.D. Bootman, H.L. Roderick, Calcium signalling: dynamics, homeostasis and remodeling, Nat. Rev. Mol. Cell. Biol. 4 (2003) 517–529.
[2] A. Divet, S. Paesante, C. Bleunven, A. Anderson, S. Treves, F. Zorzato, Novel sarco(endo)plasmic reticulum proteins and calcium homeostasis in striated muscles, J. Muscle Res. Cell Motil. 26 (2005) 7–12.
[3] H. Takeshima, S. Komazaki, M. Nishi, M. Iino, K. Kangawa, Junctophilins: a novel family of junctional membrane complex proteins, Mol. Cell 6 (2000) 11–22.
[4] K. Ito, S. Komazaki, K. Sasamoto, M. Yoshida, M. Nishi, K. Kitamura, H. Takeshima, Deficiency of triad junction and contraction in mutant skeletal muscle lacking junctophilin type 1, J. Cell Biol. 154 (2001) 1059–1068.
[5] S. Komazaki, M. Nishi, H. Takeshima, Abnormal junctional membrane structures in cardiac myocytes expressing ectopic junctophilin type 1, FEBS Lett. 542 (2003) 69–73.
[6] M. Nishi, H. Sakagami, S. Komazaki, H. Kondo, H. Takeshima, Coexpression of junctophilin type 3 and type 4 in brain, Mol. Brain Res. 110 (2003) 102–110.
[7] S. Kakizawa, Y. Kishimoto, K. Hashimoto, T. Miyazaki, K. Furutani, H. Shimizu, M. Fukaya, M. Nishi, H. Sakagami, A. Ikeda, H. Kondo, M. Kano, M. Watanabe, M. Iino, H. Takeshima, Junctophilin-mediated channel crosstalk essential for cerebellar synaptic plasticity, EMBO J. 26 (2007) 1924–1933.
[8] S. Moriguchi, M. Nishi, S. Komazaki, H. Sakagami, T. Miyazaki, H. Masumiya, S. Saito, M. Watanabe, H. Kondo, H. Yawo, K. Fukunaga, H. Takeshima, Functional uncoupling between Ca^{2+} release and afterhyperpolarization in mutant hippocampal neurons lacking junctophilins, Proc. Natl. Acad. Sci. USA 103 (2006) 10811–10816.
[9] S. Kakizawa, T. Miyazaki, D. Yanagihara, M. Iino, M. Watanabe, M. Kano, Maintenance of presynaptic function by AMPA receptor-mediated excitatory postsynaptic activity in adult brain, Proc. Natl. Acad. Sci. USA 102 (2005) 19180–19185.
[10] T. Miyazaki, K. Hashimoto, A. Uda, H. Sakagami, Y. Nakamura, S. Saito, M. Nishi, H. Kume, A. Tohgo, I. Kaneko, H. Kondo, K. Fukunaga, M. Kano, M. Watanabe, H. Takeshima, Disturbance of cerebellar synaptic maturation in mutant mice lacking BSRPs, a novel brain-specific receptor-like protein family, FEBS Lett. 580 (2006) 4057–4064.
[11] T. Miyazaki, K. Hashimoto, H.S. Shin, M. Kano, M. Watanabe, P/Q-type Ca^{2+} channel alpha 1A regulates synaptic competition on developing cerebellar Purkinje cells, J. Neurosci. 24 (2004) 1734–1743.
[12] R.A. Irizarry, B.M. Bolstad, F. Collin, L.M. Cope, B. Hobbs, T.P. Speed, Summaries of Affymetrix GeneChip probe level data, Nucleic Acids Res. 31 (2003) e15.
[13] M. Ito, Cerebellar circuitry as a neuronal machine, Prog. Neurobiol. 78 (2006) 272–303.
[14] M. Coesmans, J.T. Weber, C.I. De Zeeuw, C. Hansel, Bidirectional parallel fiber plasticity in the cerebellum under climbing fiber control, Neuron 44 (2004) 691–700.
[15] J.T. Weber, C.I. De Zeeuw, D.J. Linden, C. Hansel, Long-term depression of climbing fiber-evoked calcium transients in

Purkinje cell dendrites, Proc. Natl. Acad. Sci. USA 100 (2003) 2878–2883.
[16] M.T. Schmolesky, J.T. Weber, C.I. De Zeeuw, C. Hansel, The making of a complex spike: ionic composition and plasticity, Annu. N. Y. Acad. Sci. 978 (2002) 359–390.
[17] M. Kano, K. Hashimoto, C. Chen, A. Abeliovich, A. Aiba, H. Kurihara, M. Watanabe, Y. Inoue, S. Tonegawa, Impaired synapse elimination during cerebellar development in PKCγ mutant mice, Cell 83 (1995) 1223–1231.
[18] M.W. Jones, M.L. Errington, P.J. French, A. Fine, T.V. Bliss, S. Garel, P. Charnay, B. Bozon, S. Laroche, S. Davis, A requirement for the immediate early gene Zif268 in the expression of late LTP and long-term memories, Nat. Neurosci. 4 (2001) 289–296.

Available online at www.sciencedirect.com
ScienceDirect
ELSEVIER
Biochemical and Biophysical Research Communications 362 (2007) 971–975
BBRC
www.elsevier.com/locate/ybbrc

Augmentation of drug-induced cell death by ER protein BRI3BP

Tetsuo Yamazaki [a,b,*], Nozomi Sasaki [a,b], Miyuki Nishi [b], Daiju Yamazaki [b], Atsushi Ikeda [b], Yasushi Okuno [c], Shinji Komazaki [d], Hiroshi Takeshima [b]

[a] *The 21st Century Center of Excellence Program, Tohoku University Graduate School of Medicine, Sendai 980-8575, Japan*
[b] *Department of Biological Chemistry, Graduate School of Pharmaceutical Sciences, Kyoto University, Kyoto 606-8501, Japan*
[c] *Department of Genomic Drug Discovery Science, Graduate School of Pharmaceutical Sciences, Kyoto University, Kyoto 606-8501, Japan*
[d] *Department of Anatomy, Saitama Medical University, Saitama 350-0495, Japan*

Received 14 August 2007
Available online 27 August 2007

Abstract

To determine the contribution of the endoplasmic reticulum (ER) to cell fate decision, we focused on BRI3-binding protein (BRI3BP) residing in this organelle. BRI3BP, when overexpressed, augmented the apoptosis of human embryonic kidney 293T cells challenged with drugs including the anti-cancer agent etoposide. In contrast, the knockdown of BRI3BP reduced the drug-triggered apoptosis. BRI3BP overexpression enhanced both mitochondrial cytochrome *c* release and caspase-3 activity in etoposide-treated cells. In response to etoposide, the ER reorganized into irregularly shaped lamellae in mock-transfected cells, whereas in BRI3BP-overexpressing cells, such reorganization was not observed. These observations suggest that BRI3BP is involved in the structural dynamics of the ER and affects mitochondrial viability. Taken together, BRI3BP, widely expressed in animal cell types, seems to possess a pro-apoptotic property and can potentiate drug-induced apoptosis.

Keywords: Apoptosis; Cytochrome *c*; Endoplasmic reticulum; Etoposide; BRI3BP; Mitochondria

The endoplasmic reticulum (ER) is a multifaceted organelle. It plays a major role in protein synthesis, folding and processing. In addition to its housekeeping functions, the ER emits signals to maintain cellular homeostasis. The accumulation of structurally defective proteins in the ER initiates stress responses, which are collectively referred to as the "unfolded protein response (UPR)" [1,2]. By enhancing the ERs capacity to refold and degrade aberrant proteins, the UPR initially operates in favor of cellular survival. In contrast, cell death is induced by the UPR when the cells are exposed to excessive and prolonged ER stress. The importance of the stress response has been demonstrated also in the pathogenesis of various diseases including ischemic/reperfusion injury, neurodegenerative diseases and diabetes [3]. Toward a better understanding of such pathophysiological signals, it is necessary to identify and characterize the signaling proteins transmitting ER information to the cytoplasm.

In this work, we focused on an ER-resident protein, BRI3-binding protein (BRI3BP) [4,5]. On the basis of the results obtained, we propose that BRI3BP contributes to cell fate decision by mediating joint activities between the ER and mitochondria.

Methods

Transfection and pharmacological treatment. Human embryonic kidney 293T (293T) cells were grown in DMEM (WAKO, Tokyo, Japan) supplemented with 10% fetal calf serum (FCS) at 37 °C in a 5% CO_2 humidified incubator. For overexpression, the cDNA fragment encoding human BRI3BP or murine calumin was PCR-generated and cloned in frame into the pcDNA4/myc-His vector (Invitrogen). The pcDNA4/myc-His/lacZ vector coding for β-galactosidase was obtained from Clontech Inc. The cells were plated 16 h prior to transfection in 12-well plates at

* Corresponding author. Address: Department of Biological Chemistry, Graduate School of Pharmaceutical Sciences, Kyoto University, Kyoto 606-8501, Japan. Fax: +81 75 753 4605.
E-mail address: yamazakt@pharm.kyoto-u.ac.jp (T. Yamazaki).

0006-291X/$ - see front matter © 2007 Elsevier Inc. All rights reserved.
doi:10.1016/j.bbrc.2007.08.082

1×10^5 cells per well. The expression construct was transfected into the cells using Lipofectamine 2000 (Invitrogen). At 30 h posttransfection, etoposide (Etop), thapsigargin (Tg), and tunicamycin (Tu) (all from WAKO) were added to the culture medium. The cells were incubated for a further 40 h and then examined flow cytometrically. For BRI3BP depletion, the following small interfering RNA (siRNA) duplex obtained from Dharmacon was transfected into 293T cells using X-tremeGENE siRNA transfection reagent (Roche): 5′-gcucuuggauguucuuggauu-3′ and 5′-uccaagaacauccaagagcuu-3′. Depletion of BRI3BP mRNA was confirmed by reverse transcription polymerase chain reaction (RT-PCR) using cDNAs, synthesized with PrimeScript reverse transcriptase (Takara Bio, Shiga, Japan), as templates. The following primers were used: for BRI3BP, 5′-GCGTCGACACCATGGGCGCGCGCGCCTCAGGCGG GC-3′ and 5′-GCGAATTCTACTTGTCCTTGGAGCGGTCCAGGC TC-3′, and for β-actin, 5′-GCATTGCTGACAGGATGCAG-3′ and 5′-CCTGCTTGCTGATCCACATC-3′. The siRNA-transfected cells were split onto another 12-well plate at 72 h posttransfection. After 16 h, the cells were chemically challenged as descried above and analyzed.

Cell viability and caspase-3 activity assay. Cell viability was determined as described previously [6]. To examine caspase-3 activation, the transfected cells were treated with either dimethyl sulfoxide (vehicle) or Etop in the presence or absence of the cell-permeable pan-caspase inhibitor Z-VAD-fmk (BD Bioscience). Subsequently, caspase-3 activity was measured by flow cytometry using the CaspGLOW fluorescein active capase-3 staining kit (Medical & Biological Lab., Nagano, Japan) according to the manufacturer's instructions.

Mitochondrial cytochrome c release and transmembrane potential. Mitochondrial cytochrome *c* content was measured as described previously [7], except that the secondary antibody used was coupled with Alexa Fluor 488 instead of phycoerythrin. For examining the mitochondrial membrane potential, pharmacologically treated 293T cells were incubated for 30 min with DMEM supplemented with 10% FCS and 1 μg/ml rhodamine 123 (Rh123) in a 5% CO_2 humidified incubator, washed with PBS, and subjected to flow cytometry.

Immunoblotting. For the immunoblotting of whole cell lysates, transfected 293T cells were lyzed at 24 h posttransfection in RIPA buffer (10 mM Tris–HCl (pH 7.6), 150 mM NaCl, 2 mM EDTA, 1% Triton X-100 and 1% sodium deoxycholate, protease inhibitor cocktail (Nacalai Tesque, Tokyo, Japan)). The antibodies against the following proteins were used: BAK, BAX, Bcl-2, Bcl-X_L and actin (Santa Cruz Biotech.), and GRP78 (Abcam). BRI3BP antiserum was produced by injecting rabbits with a glutathione *S*-transferase fusion protein containing amino acids 203–253 of murine BRI3BP.

Ultrastructural analysis. The pharmacologically treated cells were prepared for electron microscopy study as described previously [8].

Statistics. Statistical significance was evaluated using Student's *t* test unless otherwise mentioned.

Results

Facilitation of drug-induced apoptosis by BRI3BP overexpression

The localization of BRI3BP to both the ER and the nuclear membrane prompted us to explore the possibility that BRI3BP is involved in signaling from the ER. To this end, 293T cells transfected with human BRI3BP that was fused to the mycHis tag (Suppl. Fig. 1A and B) were incubated with apoptosis inducers including ER stressors such as Tg (sarcoplasmic/endoplasmic Ca^{2+}–ATPase inhibitor) and Tu (*N*-glycosylation inhibitor), and the chemotherapy drug Etop (topoisomerase II inhibitor). The cells were probed using a combination of fluorescein isothiocyanate-coupled Annexin V (Annexin V-FITC) and the DNA-specific fluorochrome 7-amino-actinomycin D (7-AAD) to simultaneously determine phosphatidyl serine exposure and plasma membrane permeability by flow cytometry [9,10]. Subsequently, cell subsets undergoing early (Annexin V^+/7-AAD^-) and late (Annexin V^+/7-AAD^+) apoptosis were quantified (Suppl. Fig. 1C). BRI3BP transfection led to a 15–30% increase in apoptosis compared with mock transfection. On the other hand, no obvious effects of β-galactosidase (cytosolic protein) and calumin (ER transmembrane protein [6]) on apoptosis were detected (Suppl. Fig. 1D), suggesting that BRI3BP specifically enhances drug-initiated apoptosis. Increased vulnerability to the pharmacological insults was corroborated over a wide range of drug concentrations (Fig. 1A).

Reduction of drug-induced apoptosis by BRI3BP depletion

We further investigated the role of BRI3BP using an siRNA-mediated knockdown approach. Transfection of an siRNA duplex corresponding to the BRI3BP open reading frame, but not to a scrambled (Sc) sequence, resulted in a marked decrease in the levels of BRI3BP mRNA and protein, as shown by RT-PCR and immunoblotting,

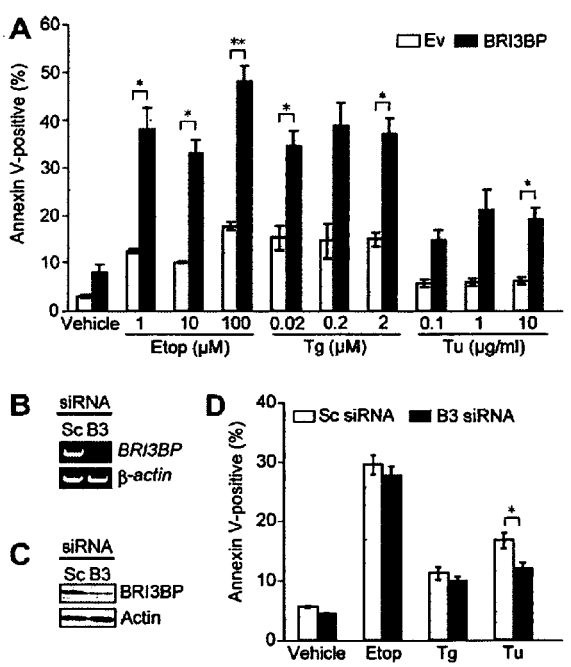

Fig. 1. Enhancement of drug-induced apoptosis by BRI3BP. (A) 293T cells transfected with either an empty vector (Ev) or the plasmid encoding the mycHis-tagged BRI3BP (BRI3BP) were pharmacologically treated for flow cytometric analysis. Annexin V positivity indicates the total percentage of two subpopulations (Annexin V^+/7-AAD^- and Annexin V^+/7-AAD^+). The result represents mean ± SEM of five separate experiments. $^*P < 0.05$, $^{**}P < 0.01$. (B,C) 293T cells were transiently transfected with siRNA duplexes for either BRI3BP (B3) or an irrelevant sequence (Sc), followed by RT-PCR and immunoblotting. (D) The siRNA-transfected cells were challenged with the vehicle, 100 μM Etop, 2 μM Tg or 10 μg/ml Tu for flow cytometry. The result represents mean ± SEM of five independent experiments. $^*P < 0.05$.

respectively (Fig. 1B and C). Tu-induced apoptosis was mitigated by BRI3BP depletion (Fig. 1D). On the other hand, apoptosis triggered by either Etop or Tg was marginally affected. Although the signaling pathways each drug utilizes for triggering apoptosis have not been elucidated in detail, death-signal cascades activated by Etop/Tg seem to be less BRI3BP-dependent than those activated by Tu. Taken together, the observed correlation between the abundance of BRI3BP and the vulnerability to pharmacological insults suggests that BRI3BP is involved in apoptosis-inducing signals emanating from the ER.

Enhanced activation of the caspase cascade by BRI3BP

We then investigated whether BRI3BP exploited the ordinary caspase signaling pathway [11] in enhancing the pharmacologically induced apoptosis of 293T cells. Because the pro-apoptotic property of BRI3BP became most clear upon treatment of the cells with Etop rather than with Tg or Tu, we analyzed the cells incubated with Etop with or without the cell-permeable pan-caspase inhibitor Z-VAD-fmk. Annexin V positivity determined by flow cytometry was decreased with Z-VAD-fmk, regardless of whether BRI3BP was transfected into the cells (Suppl. Fig. 2A). Correspondingly, the inhibitor reduced the activity of caspase-3, an effector caspase, in the Etop-treated cells as demonstrated by decreased signals derived from FITC-coupled DEVD-fmk, which irreversibly binds to activated caspase-3 (Suppl. Fig. 2B). The overexpression of BRI3BP, therefore, increases the sensitivity to Etop by upregulating the caspase cascade.

Mitochondrial damage induced by BRI3BP

The caspase-dependent facilitation of Etop-induced apoptosis by BRI3BP prompted us to examine which level along the caspase signaling pathway was modulated. The liberation of cytochrome *c* from the mitochondrial intermembrane space initiates apoptosome formation and culminates in the activation of effector caspases including caspase-3 [12,13]. Because chemotherapeutic agents trigger the mitochondrial release of cytochrome *c*, we hypothesized that this might be the step BRI3BP promoted in rendering the cells highly sensitive to Etop. The quantitation of mitochondrial cytochrome *c* content by flow cytometry revealed that BRI3BP overexpression induced an increase in the percentage of cytochrome *c*-negative subsets upon Etop treatment, indicating enhanced cytochrome *c* release (Fig. 2A). We further assessed the mitochondrial transmembrane potential ($\Delta\Psi_m$) using the membrane-permeable lipophilic cationic fluorochrome rhodamine 123 (Rh123) as a probe [9]. In response to Etop, BRI3BP-transfected cells showed $\Delta\Psi_m$ dissipation to a greater degree than mock-transfected control cells (Fig. 2B). Deterioration in mitochondrial functions, represented by both cytochrome *c* release and $\Delta\Psi_m$ collapse, is known to be closely associated with an imbalance between pro- and anti-apoptotic Bcl-2

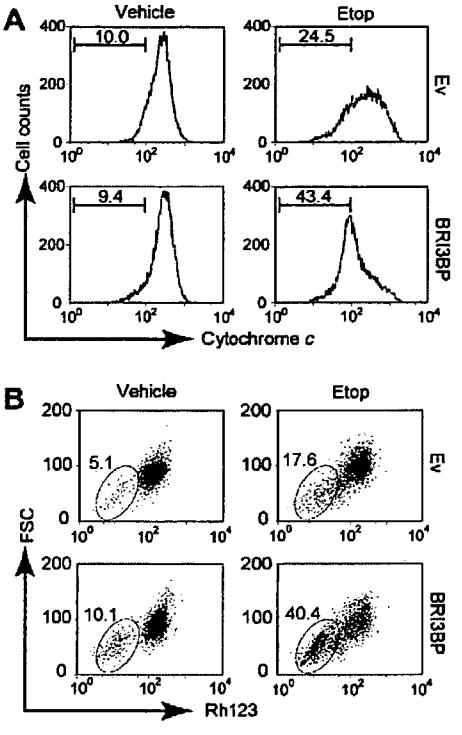

Fig. 2. Impairment of mitochondrial membrane integrity by BRI3BP overexpression. Transfected 293T cells challenged with 100 μM Etop were subjected to flow cytometric analysis of mitochondrial cytochrome *c* content (A) and transmembrane potential (B). FSC, forward light scatter. Experiments were repeated three times with similar results.

family members [14–16]. Immunoblot analysis detected no significant alterations in the expression levels of major Bcl-2 family proteins in BRI3BP-transfected cells (Suppl. Fig. 3), indicating that BRI3BP does not tip the balance, at least quantitatively, among the family members. Collectively, mitochondrial dysfunction underlies the priming of 293T cells by BRI3BP for Etop-induced apoptosis.

Absence of Etop-induced ER reorganization upon BRI3BP overexpression

Mitochondria lie adjacent to and operate in concert with the ER [17–19]. We then explored by electron microscopy the possibility that the mitochondrial dysfunction observed was secondary to the defects in the ER, where BRI3BP is localized. Treatment with the vehicle alone did not lead to a clear difference in ER morphology between mock- and BRI3BP-transfected 293T cells (Fig. 3A, B, E, and G). Upon exposure to Etop, the ER in the mock-transfected cells underwent morphological changes. It appeared in sections as whorls or a convoluted lamellar structure continuous with the nuclear membrane, to which mitochondria was frequently apposed (Fig. 3F). In contrast, such ER restructuring induced by Etop was effectively suppressed in the BRI3BP-overexpressing cells and the ER extending directly from the nuclear membrane was barely observed

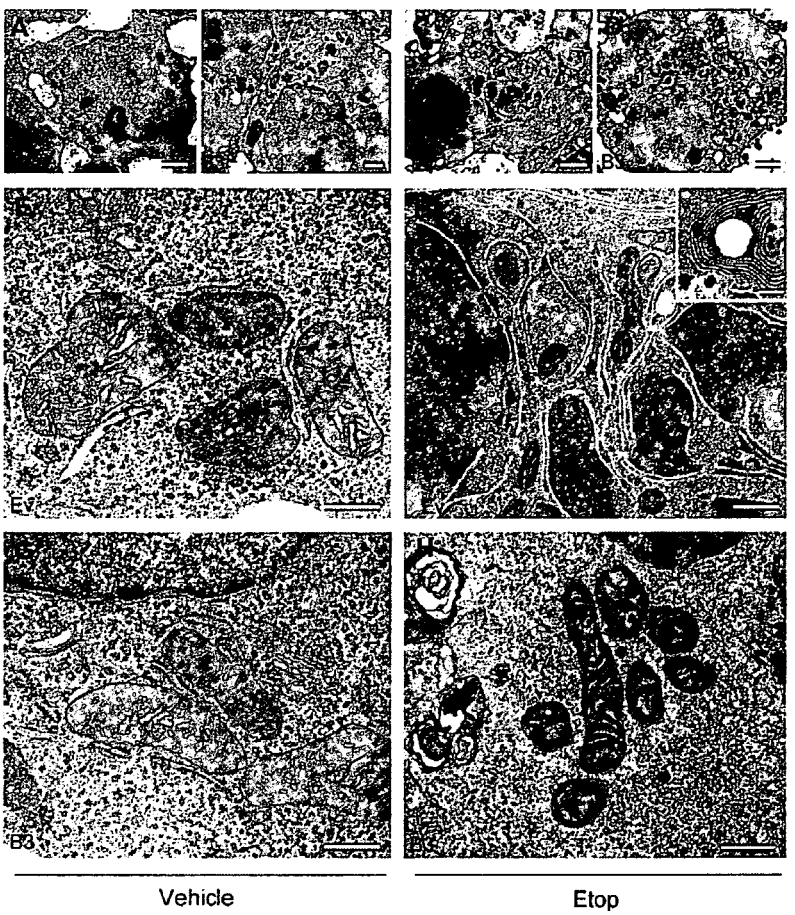

Fig. 3. Lack of ER transformation in BRI3BP-transfected 293T cells. The mock (Ev)- and the BRI3BP (B3)-transfected cells were treated with the vehicle (A,B,E,G) or 100 μM Etop (C,D,F,H) for electron microscopy. Bars, 2 μm (A–D); 0.5 μm (E–H). Data shown represent three separate experiments.

(Fig. 3H). In addition, structurally damaged mitochondria were more readily detected upon BRI3BP overexpression (Fig. 3C and D). These data suggest that the enforced expression of BRI3BP downregulates the structural plasticity of the ER, which is potentially linked to mitochondrial viability.

Discussion

In this report, we found that the BRI3BP transfection facilitates drug-induced apoptosis. It has been known that the overproduction of integral membrane proteins triggers the ER-overload response [20]. It is thus possible that the potentiation of pharmacologically induced apoptosis upon BRI3BP overexpression is attributable primarily to the excessive ER stress, but not to the specific action inherent to BRI3BP itself. However, this possibility is not supported by our data that GRP78, a chaperon induced by ER stress, was below the detection limit in both mock- and BRI3BP-transfected cells treated with either the vehicle or Etop (Suppl. Fig. 4). Therefore, in addition to BRI3BP overexpression, cofactors are required for facilitating apoptosis. This view is further supported by the fact that BRI3BP transfection alone did not induce mitochondrial dysfunction (Fig. 2).

The ER elements have various morphological forms [21,22]. It is an attractive hypothesis that the structural shift of the ER could represent a cellular adaptive response that serves to minimize the propagation of cell death signals from the ER. Because the BRI3BP overexpression inhibited Etop-induced ER restructuring (Fig. 3), it can be assumed that the facilitation of Etop-triggered apoptosis is due to the impaired plasticity of ER morphology. Major protein components of the nuclear membrane undergo caspase-dependent proteolysis in Etop-challenged cells [23]. It is therefore hypothesized that the physiological functions of the nuclear membrane are severely perturbed in BRI3BP-overexpressing cells, which showed the enhanced caspase-3 activity in response to Etop. As a result, the ER, which is structurally continuous with the nuclear membrane, might be unable to reorganize in this setting.

In this report, the relationship between the BRI3BP level and cell survival/death was analyzed *in vitro* using a cell line challenged with apoptosis inducers. If this relationship holds true *in vivo*, a reduction or loss of BRI3BP might result in the inefficient elimination of harmful cells, favoring tumor development. The array-based analysis

has demonstrated that BRI3BP mRNA levels are lower in human tumor samples (Suppl. Fig. 5), suggesting the involvement of BRI3BP in cell fate decision under physiological conditions. It is therefore possible that the BRI3BP expression level is associated with pathogenesis and that BRI3BP is a potential target of pharmacological intervention.

Acknowledgments

We are grateful to Prof. Kazuo Sugamura for continuous encouragement. This work was supported in part by grants from the Ministry of Education, Culture, Sports, Science, and Technology of Japan, the Naito Foundation, the Sumitomo Foundation, the Life Science Foundation, the Takeda Science Foundation, the Uehara Memorial Foundation, and the 21st Century Center of Excellence program.

Appendix A. Supplementary data

Supplementary data associated with this article can be found, in the online version, at doi:10.1016/j.bbrc.2007.08.082.

References

[1] R.J. Kaufman, Stress signaling from the lumen of the endoplasmic reticulum: coordination of gene transcriptional and translational controls, Genes Dev. 13 (1999) 1211–1233.
[2] D. Ron, P. Walter, Signal integration in the endoplasmic reticulum unfolded protein response, Nat. Rev. Mol. Cell Biol. 8 (2007) 519–529.
[3] C. Xu, B. Bailly-Maitre, J.C. Reed, Endoplasmic reticulum stress: cell life and death decisions, J. Clin. Invest. 115 (2005) 2656–2664.
[4] L. Lin, Y. Wu, C. Li, S. Zhao, Cloning, tissue expression pattern, and chromosome location of a novel human gene BRI3BP, Biochem. Genet. 39 (2001) 369–377.
[5] T. Katahira, Y. Imamura, D. Kitamura, The BASH/BLNK/SLP-65-associated protein BNAS1 regulates antigen-receptor signal transmission in B cells, Int. Immunol. 18 (2006) 545–553.
[6] M. Zhang, T. Yamazaki, M. Yazawa, S. Treves, M. Nishi, M. Murai, E. Shibata, F. Zorzato, H. Takeshima, Calumin, a novel Ca^{2+}-binding transmembrane protein on the endoplasmic reticulum, Cell Calcium 42 (2007) 83–90.
[7] N.J. Waterhouse, J.A. Trapani, A new quantitative assay for cytochrome *c* release in apoptotic cells, Cell Death Differ. 10 (2003) 853–855.
[8] H. Takeshima, S. Komazaki, K. Hirose, M. Nishi, T. Noda, M. Iino, Embryonic lethality and abnormal cardiac myocytes in mice lacking ryanodine receptor type 2, EMBO J. 17 (1998) 3309–3316.
[9] E. Bedner, X. Li, W. Gorczyca, M.R. Melamed, Z. Darzynkiewicz, Analysis of apoptosis by laser scanning cytometry, Cytometry 35 (1999) 181–195.
[10] I. Vermes, C. Haanen, C. Reutelingsperger, Flow cytometry of apoptotic cell death, J. Immunol. Methods 243 (2000) 167–190.
[11] I.N. Lavrik, A. Golks, P.H. Krammer, Caspases: pharmacological manipulation of cell death, J. Clin. Invest. 115 (2005) 2665–2672.
[12] D.R. Green, G. Kroemer, The pathophysiology of mitochondrial cell death, Science 305 (2004) 626–629.
[13] G. Kroemer, L. Galluzzi, C. Brenner, Mitochondrial membrane permeabilization in cell death, Physiol. Rev. 87 (2007) 99–163.
[14] J.M. Adams, Ways of dying: multiple pathways to apoptosis, Genes Dev. 17 (2003) 2481–2495.
[15] J.C. Reed, Proapoptotic multidomain Bcl-2/Bax-family proteins: mechanisms, physiological roles, and therapeutic opportunities, Cell Death Differ. 13 (2006) 1378–1386.
[16] M.F. van Delft, D.C.S. Huang, How the Bcl-2 family of proteins interact to regulate apoptosis, Cell Res. 16 (2006) 203–213.
[17] R. Rizzuto, P. Pinton, W. Carrington, F.S. Fay, K.E. Fogarty, L.M. Lifshitz, R.A. Tuft, T. Pozzan, Close contacts with the endoplasmic reticulum as determinants of mitochondrial Ca^{2+} responses, Science 280 (1998) 1763–1766.
[18] L. Scorrano, S.A. Oakes, J.T. Opferman, E.H. Cheng, M.D. Sorcinelli, T. Pozzan, S.J. Korsmeyer, BAX and BAK regulation of endoplasmic reticulum Ca^{2+}: a control point for apoptosis, Science 300 (2003) 135–139.
[19] G. Csordas, C. Renken, P. Varnai, L. Walter, D. Weaver, K.F. Buttle, T. Balla, C.A. Mannella, G. Hajnoczky, Structural and functional features and significance of the physical linkage between ER and mitochondria, J. Cell Biol. 174 (2006) 915–921.
[20] H.L. Pahl, P.A. Baeuerle, The ER-overload response: activation of NF-κB, Trends Biochem. Sci. 22 (1997) 63–67.
[21] C.M. Federovitch, D. Ron, R.Y. Hampton, The dynamic ER: experimental approaches and current questions, Curr. Opin. Cell Biol. 17 (2005) 409–414.
[22] N. Borgese, M. Francolini, E. Snapp, Endoplasmic reticulum architecture: structures in flux, Curr. Opin. Cell Biol. 18 (2006) 358–364.
[23] B. Buendia, A. Santa-Maria, J.C. Courvalin, Caspase-dependent proteolysis of integral and peripheral proteins of nuclear membranes and nuclear pore complex proteins during apoptosis, J. Cell Sci. 112 (1999) 1743–1753.

MOLECULAR AND CELLULAR BIOLOGY, Apr. 2007, p. 3008–3022 Vol. 27, No. 8
0270-7306/07/$08.00+0 doi:10.1128/MCB.02047-06

Germinal Center Marker GL7 Probes Activation-Dependent Repression of *N*-Glycolylneuraminic Acid, a Sialic Acid Species Involved in the Negative Modulation of B-Cell Activation▽†

Yuko Naito,[1,7] Hiromu Takematsu,[1,7] Susumu Koyama,[2] Shizu Miyake,[2] Harumi Yamamoto,[5] Reiko Fujinawa,[5] Manabu Sugai,[4] Yasushi Okuno,[3] Gozoh Tsujimoto,[3] Toshiyuki Yamaji,[5] Yasuhiro Hashimoto,[5,7] Shigeyoshi Itohara,[6] Toshisuke Kawasaki,[2]‡ Akemi Suzuki,[5] and Yasunori Kozutsumi[1,5,7]*

Laboratory of Membrane Biochemistry and Biophysics, Graduate School of Biostudies,[1] Department of Biological Chemistry,[2] and Department of Genomic Drug Discovery, Graduate School of Pharmaceutical Sciences,[3] and Center for Genomic Medicine, Graduate School of Medicine,[4] Kyoto University, Sakyo, Kyoto 606-8501, Japan; Supra-Biomolecular System Research Group, RIKEN Frontier Research System,[5] and Laboratory for Behavioral Genetics, RIKEN Brain Science Institute,[6] RIKEN, Wako, Saitama 351-0198, Japan; and CREST, Japan Science and Technology, Kawaguchi, Saitama, Japan[7]

Received 2 November 2006/Returned for modification 9 January 2007/Accepted 30 January 2007

Sialic acid (Sia) is a family of acidic nine-carbon sugars that occupies the nonreducing terminus of glycan chains. Diversity of Sia is achieved by variation in the linkage to the underlying sugar and modification of the Sia molecule. Here we identified Sia-dependent epitope specificity for GL7, a rat monoclonal antibody, to probe germinal centers upon T cell-dependent immunity. GL7 recognizes sialylated glycan(s), the α2,6-linked *N*-acetylneuraminic acid (Neu5Ac) on a lactosamine glycan chain(s), in both Sia modification- and Sia linkage-dependent manners. In mouse germinal center B cells, the expression of the GL7 epitope was upregulated due to the in situ repression of CMP-Neu5Ac hydroxylase (Cmah), the enzyme responsible for Sia modification of Neu5Ac to Neu5Gc. Such Cmah repression caused activation-dependent dynamic reduction of CD22 ligand expression without losing α2,6-linked sialylation in germinal centers. The in vivo function of *Cmah* was analyzed using gene-disrupted mice. Phenotypic analyses showed that Neu5Gc glycan functions as a negative regulator for B-cell activation in assays of T-cell-independent immunization response and splenic B-cell proliferation. Thus, Neu5Gc is required for optimal negative regulation, and the reaction is specifically suppressed in activated B cells, i.e., germinal center B cells.

The germinal center is a special microenvironment which occurs in secondary lymphoid organs, mainly in response to T-cell-dependent antigen immunization. Mature B cells entering the germinal center edit their immunoglobulin gene through somatic hypermutation and class-switching recombination, differentiating into memory cells and plasma cells (30, 33). The activated B cells during the germinal center reaction in mice can be probed with peanut (*Arachis hypogaea*) lectin, peanut agglutinin (PNA) (8, 37, 46), or a rat monoclonal antibody (MAb), GL7 (5). GL7 was originally reported as a marker for polyclonally activated T and B cells (28) in mice. GL7 stains a subpopulation of T cells (19) and a subpopulation of the large pre-B-cell stage during differentiation in the bone marrow (38). Activated B cells express the GL7 epitope, but mature B cells do not; thus, GL7 serves as a marker for germinal centers in the immunized spleen (18, 41, 52) or lymph nodes, and $GL7^{high}$ B cells have been shown to have higher functional activity for producing antibodies and presenting antigens (5). Despite growing knowledge about the use of this antibody as a marker for lymphocytes in various conditions, the molecular epitope of GL7 is poorly defined to date. In the original article characterizing GL7, Laszlo et al. (28) showed that GL7 could immunoprecipitate a 35-kDa cell surface protein from metabolically labeled activated B cells. However, no other studies have been published on this subject.

In the present study, we found that GL7 recognizes a glycan moiety containing terminal sialic acid (Sia) in both linkage- and modification-dependent manners. Sia is a family of acidic nine-carbon sugars that often occupies the nonreducing terminus of mammalian glycan chains (47), and Sia is essential for early development of mice (49). The localization of Sia-bearing glycan chains on the cell surface makes sialylated molecules seem to be likely targets for various cellular and molecular recognition molecules, such as the mammalian lectins that are abundant in the immune system (61). A family of enzymes, sialyltransferases, is responsible for the formation of the Sia linkage to the underlying glycan chains. To determine the

* Corresponding author. Mailing address: Laboratory of Membrane Biochemistry and Biophysics, Graduate School of Biostudies, Kyoto University, Yoshida-shimoadachi, Sakyo-ku, Kyoto 606-8501, Japan. Phone: 81 75 753 7684. Fax: 81 75 753 7686. E-mail: yasu@pharm.kyoto-u.ac.jp.

‡ Present address: Research Center for Glycobiotechnology, Ritsumeikan University, Kyoto, Japan.

† Supplemental material for this article may be found at http://mcb.asm.org/.

▽ Published ahead of print on 12 February 2007.

linkage specificity of GL7 recognition, we used the gene expression profiles of sialylation-related genes obtained by DNA microarray analysis to screen for a responsible sialyltransferase gene for the biosynthesis of the GL7 determinant.

Apart from the linkage variations, Sia also occurs in various molecular species as a result of modifications at its C-4, C-5, C-7, C-8, and C-9 positions; these modifications are spatially and temporary regulated (60). We also found that the determinant recognition by GL7 is specific to a Sia modification at the C-5 position. In mice, Sia occurs in two main forms with respect to the moiety at the C-5 position: *N*-acetylneuraminic acid (Neu5Ac), which is a precursor form of the diverse Sia family, and its major modified form, *N*-glycolylneuraminic acid (Neu5Gc). The structural difference between Neu5Ac and Neu5Gc is a single oxygen atom in the C-5 position. The modification reaction that produces Neu5Gc is catalyzed at the sugar-nucleotide level in the cytosol by the enzyme CMP-Neu5Ac hydroxylase (Cmah) (24, 53). Cmah determines the cell surface expression ratio of these two Sia species, as the cytosolic Cmah reaction occurs prior to the sialyltransferase reaction, which takes place in the Golgi apparatus during the biosynthesis of glycoconjugates. We found that GL7 recognizes only Neu5Ac-bearing glycans and that the reduction of *Cmah* expression plays a major role in the formation of the GL7 epitope in activated B cells in the germinal center, which was in sharp contrast to the dominant expression of Neu5Gc in mouse lymphocytes.

To examine the in vivo function of Neu5Gc-bearing glycans, we disrupted the *Cmah* gene in mice. *Cmah* disruption is expected to modify the Sia-mediated Sia species-specific recognition event without affecting overall sialylation, which can affect the behavior of the protein in various ways. We primarily focused on the phenotypic consequences of *Cmah* disruption in B cells since Cmah is regulated in B cells, especially in response to activation. *Cmah*-null mice exhibited hyperresponsive B cell phenotypes in assays measuring B-cell functions, i.e., antibody production and proliferation.

MATERIALS AND METHODS

Materials. Most of the materials used were obtained from Wako Chemical (Osaka, Japan) or Nacalai Tesque (Kyoto, Japan). The human immunoglobulin G1 (IgG1)-Fc fusion construct was provided by Paul Crocker and Ajit Varki. The Lec2 cells were provided by Pamela Stanley. The Plat-E cells were provided by Toshio Kitamura. Human B-cell lines were obtained from the Japanese Collection of Research Bioresources.

Antibodies and lectins. The antibodies used were as follows: donkey $F(ab')_2$ against mouse IgM (Jackson ImmunoResearch, West Grove, PA); R-phycoerythrin (R-PE)-conjugated anti-mouse B220 (RA3-6B2); R-PE-conjugated goat $F(ab')_2$ anti-human IgG-Fc; R-PE-conjugated streptavidin (CALTAG Laboratories, Burlingame, CA); fluorescein isothiocyanate (FITC)-conjugated and purified GL7; FITC-conjugated anti-mouse B220 (RA3-6B2); R-PE-conjugated anti-mouse I-A/I-E (M5/114.15.2); biotin-conjugated anti-CD22 (Cy34.1) (BD Pharmingen, San Diego, CA); horseradish peroxidase (HRP)-conjugated goat anti-rat IgM; alkaline phosphatase-conjugated isotype-specific goat anti-mouse IgA, IgG1, IgG3, and IgM; unlabeled isotype-specific goat anti-mouse IgA and IgG3; R-PE-conjugated anti-mouse IgM (1B4B1); biotin-conjugated anti-mouse CD22 (2D6) (Southern Biotechnology Associates, AL); anti-mouse polyvalent Igs; HRP-conjugated PT-66 (an antiphosphotyrosine MAb; Sigma, St. Louis, MO); CD90 (Thy1.2) MicroBeads; anti-FITC MicroBeads (Miltenyi Biotec, Bergisch Gladbach, Germany); rabbit anti-mouse CD22 serum (Chemicon, Temecula, CA), HRP-conjugated donkey $F(ab')_2$ anti-rabbit Ig (Amersham Life Science, Buckinghamshire, United Kingdom); antiactin (Santa Cruz Biotechnology, Santa Cruz, CA); HRP-conjugated goat anti-mouse IgG; HRP-conjugated rabbit anti-goat IgG (ZYMED Lab, South San Francisco, CA). Anti-CD22 MAb (Cy34.1) was purified from the culture supernatant of hybridoma Cy34.1 (ATCC). Biotinylated *A. hypogaea* PNA was obtained from HONEN (Tokyo, Japan), and FITC-conjugated *Sambucus sieboldiana* agglutinin (SSA) was obtained from Seikagaku Kogyo (Tokyo, Japan).

Preparation of Fc fusion proteins of sialoadhesin and CD22. Recombinant soluble forms of the amino-terminal domains (domains 1 to 3) of mouse sialoadhesin/Siglec-1, mouse CD22/Siglec-2, and human CD22/Siglec-2 fused to the Fc region of human IgG1 (mSn-Fc, mCD22-Fc, and hCD22-Fc, respectively) were produced in stably transfected Lec2 cells, a cell line deficient in protein sialylation. The production of the Siglec (Sia-binding Ig superfamily lectin)-Fc fusion probe in the Lec2 cell line resulted in considerably enhanced binding to the ligand, which allowed the identification of changes in ligand expression. The Siglec-Fc probes were purified from the culture supernatant using protein A-Sepharose columns (Pierce, Rockford, IL).

Flow cytometry. Cell labeling was carried out in fluorescence-activated cell sorter buffer (1% bovine serum albumin [BSA] and 0.1% NaN_3 in phosphate-buffered saline [PBS]). Data were acquired using a FACScan (Becton Dickinson, Franklin Lakes, NJ) instrument and analyzed using FlowJo software (Tree Star, San Carlos, CA). For comparison with the microarray data, B lymphoma cells (1×10^5) were stained with FITC-conjugated GL7 (dilution, 1:100) for 1 h. This staining condition was determined using the criterion that the strongest staining did not reach a plateau. Mean fluorescence intensity (MFI) of GL7 staining was acquired using a FACScan at settings under which unstained control cells gave a signal of around 5 on the FL-1 channel. The mean FL-1 signal of each stained sample was divided by that of the unstained sample to produce the relative staining profiles on flow cytometry to be compared with the cDNA microarray profiles of relative gene expression. For mSn-Fc, mCD22-Fc, and hCD22-Fc staining, these Fc fusion proteins were precomplexed with R-PE-conjugated goat $F(ab')_2$ anti-human IgG.

Sialidase treatment. Sialidase treatment was carried out in 100 mM sodium acetate (pH 5.2) for 30 min at room temperature prior to the staining for flow cytometry. Sialidase from *Arthrobacter ureafaciens* (Calbiochem, San Diego, CA) and sialidase from *Salmonella enterica* serovar Typhimurium (Takara, Kusatsu, Japan) were used.

Immunoblotting with GL7. The cells were sonicated in detergent-free lysis buffer (25 mM Tris-HCl [pH 7.6], 1 mM dithiothreitol, protease inhibitor cocktail [Nacalai Tesque]). The pellets (membrane fractions) were collected by ultracentrifugation and solubilized in NP-40 lysis buffer (1% Nonidet P-40, 150 mM NaCl, 25 mM HEPES [pH 7.4], protease inhibitor cocktail). The extracts were subjected to immunoblotting with GL7 in the presence or absence of 100 mM Neu5Ac.

Development of cDNA microarray for glycan-related genes. The RIKEN Frontier Human Glyco-gene cDNA microarray, version 2, which was spotted by Takara, consisted of 888 genes, which included glycosyltransferase genes and genes related to sugar metabolism, glycan modification, glycan recognition, and lipid metabolism.

Use of cDNA microarray for identification of glycan-related genes. $Poly(A)^+$ RNA samples were isolated from mid-log-phase cells using the mTRAP system (Activemotif, Carlsbad, CA) and were quality checked using a Bioanalyzer 2100 (Agilent Technologies, Santa Clara, CA). One microgram of $poly(A)^+$ RNA from the B-cell lines (rRNA contamination subtracted) and universal reference RNA (Clontech, Mountain View, CA) were labeled using a CyScribe first-strand cDNA labeling kit (Amersham). Competitive hybridization was performed on the microarray, and data were obtained using an Affymetrix 428 array scanner. To achieve a fair cross-cell line comparison, we fixed Cy3 as the signal for the universal reference RNA and Cy5 for the RNA from the B-cell lines. Microarray data were background corrected using a smoothing function and then Lowess normalized using linear models for microarray data. This readout was sigma normalized to avoid variation among microarray replicates. Then, the Cy5 signal from the B-cell lines was divided by the Cy3 signal to obtain the relative expression profile for each gene in the six cell lines as expression ratios relative to the universal reference RNA (1, 16, 29, 40). The gene expression profiles were compared with the GL7 staining profiles from flow cytometry. The similarity between the profiles was evaluated with Pearson's correlation coefficient, and probability values (*P* values) were calculated by the correlation coefficient test. For the correlation coefficient test of a sample size of six, a coefficient of 0.81 indicates a statistical significance level of 5%.

Transfection. CHO-K1 cells were stably transfected with pIRES (where IRES is internal ribosome entry site) vector (Clontech), either with or without rat cDNA for *St6gal1*. Transfected cells were selected with G418 (1 mg/ml), and multiple stable clones were established.

Enzyme-linked immunosorbent assay (ELISA). In 96-well assay plates, GL7 antibody was immobilized in wells coated with the capturing antibody, purified

anti-rat IgM. The wells were washed and incubated with streptavidin-conjugated sugar chain probes (50 μM), prepared as previously reported (65). The captured probes were detected with biotinylated alkaline phosphatase (Vector Laboratories, Burlingame, CA) and *p*-nitrophenyl phosphate by measuring the absorbance at 405 nm.

Spleen sectioning and immunohistochemistry. Mice were immunized intraperitoneally with 3×10^8 sheep red blood cells (SRBC) in 100 μl of saline. Spleens were removed 8 or 10 days after immunization and embedded in Tissue-Tek OCT (22-oxyacalcitriol) compound (Sakura Finetechnical, Tokyo, Japan). Spleen sections were cut at a 6-μm thickness on a cryostat microtome (Leica Geosystems, Heerbrugg, Switzerland), thaw-mounted onto Matsunari adhesive silane-coated slides, and fixed in acetone. After rehydration in Tris-buffered saline and blocking in Tris-buffered saline with 5% BSA and 0.05% Tween 20, the sections were stained with GL7, PNA, or mCD22-Fc precomplexed with R-PE-conjugated anti-human IgG. The stained sections were analyzed under a confocal laser-scanning microscope (Olympus, Tokyo, Japan).

Magnetic sorting preparation of splenic B-cell-enriched fraction. B-cell-enriched fractions were obtained by Thy1.2 depletion of splenocytes on a MACS (magnetic cell sorter) depletion column (Miltenyi Biotec). Thy1.2-depleted fractions were stained with B220 to confirm B-cell enrichment. To avoid Neu5Gc contamination in the experimental systems, RPMI 1640 medium (Invitrogen, Carlsbad, CA) containing 10% human serum (Uniglobe, Reseda, CA) or chicken serum (JRH Biosciences, Lenaxa, KS), rather than fetal bovine serum (FBS) (JRH), was used in most of the experiments. In addition, sodium pyruvate (Invitrogen), nonessential amino acids solution (Invitrogen), L-glutamine, and 2-mercaptoethanol were added to the medium.

Germinal center B-cell analyses. Splenic B cells from SRBC-immunized mice were incubated with FITC-conjugated GL7 and then with anti-FITC MicroBeads. The labeled cells were collected as germinal center B cells using a MACS LS column (Miltenyi Biotec). The germinal center, nongerminal center, and control (untreated) B cells were lysed by sonication in detergent-free lysis buffer (described above), and the lysates were separated by ultracentrifugation. The supernatant (cytosolic fraction) was used for immunoblotting with anti-Cmah antibody, and the pellet (membrane fraction) was used for the analysis of Sia species by high-pressure liquid chromatography (HPLC). Immunoblotting was performed using rabbit N8 antiserum against mouse Cmah, as previously reported (27). The ratios of Neu5Gc were determined by derivatizing Sia with 1,2-diamino-4,5-methylenedioxybenzene (DMB), a fluorescent compound for α-keto acids, as previously described (27). In brief, Sia was released by incubating the pellet in 2 M acetic acid at 80°C, derivatized with DMB (Dojindo, Mashiki, Japan), and analyzed on a reverse-phase column (TSK-gel ODS-80Tm; Tosoh, Tokyo, Japan) using a Shimadzu LC10 HPLC system.

Detection of Sia in tissues. The ratios of Neu5Ac and Neu5Gc were determined as above. Sia was released by incubating tissues in 100 mM sulfuric acid (which also destroys the *O*-acetyl group often found on the C-7 to C-9 positions of Sia molecules), derivatized with DMB, and analyzed by HPLC.

Real-time RT-PCR analysis. Real time reverse transcription-PCR (RT-PCR) experiments were performed using a QuantiTect SYBR Green PCR kit (QIAGEN Japan, Tokyo, Japan) and an ABI 7700 sequence detection system (Applied Biosystems Japan, Tokyo, Japan). Total RNA was purified from untreated or lipopolysaccharide (LPS)-stimulated mouse splenic B cells, and 2 μg was used for reverse transcription. The amplification cycle was as follows: 15 min at 95°C, followed by up to 40 cycles of 15 s at 94°C, 30 s at 58°C/50°C, and 30 s at 72°C. The PCR primers used for amplification were: ZP-5, 5′-AGATTTAC AAGGATTCC-3′; ZP-E, 5′-CTTAAATCCAGCCCA-3′ (*Cmah*); PS-mCD22-6, 5′-CCTCCACTCCTCAGGCCAGA-3′; PS-mCD22-E, 5′-GCCTATCCCATTG GTCCCT-3′ (*Cd22*); PS-ST6Gal-1, 5′-TCTTCGAGAAGAATATGGTG-3′; PS-ST6Gal-A, 5′-GACTTATGGAGAAGGATGAG-3′ (*St6gal1*); PS-GAPDH-1 (where GAPDH is glyceraldehyde-3-phosphate dehydrogenase), 5′-GTGGAGATTGTTGCC ATCAACG-3′; PS-GAPDH-A, 5′-TCTCGTGGTTCACACCCATCAC-3′ (*Gapdh*); PS-BACTIN-1, 5′-ACGATATCGCTGCGCTGGTC-3′; and PS-BACTIN-A, 5′-CAT GAGGTAGTCTGTCAGGT C-3′ (*Actb*). Each sample was analyzed in more than three wells. Relative mRNA abundance was calculated using the comparative cycle threshold method and expressed as a ratio to the nonstimulated sample.

Retrovirus preparation and infection. *Cmah* cDNA was cloned into the modified mouse stem cell virus vector, which expresses *Cmah* and the extracellular domain of human *CD4* by means of an internal ribosome entry site. Plasmids were transiently transfected into Plat-E packaging cells (35), and retrovirus-containing supernatants were collected. After stimulation with LPS for 12 to 14 h, splenic B cells were spin infected (at 32°C for 90 min) with the retrovirus in the presence of *N*[1-(2,3-dioleoyloxy)propyl]-*N*,*N*,*N*-trimethylammonium methylsulfate (DOTAP; Roche Diagnostics, Mannheim, Germany). The retrovirus-infected B cells were cultured in the presence of 30 μg/ml LPS for 2 to 2.5 days, and then human CD4-positive cells were enriched with a MACS system using MACSelect 4 MicroBeads (Miltenyi Biotec). The sorted cells were subjected to flow cytometry or a proliferation assay (described below).

Targeting construct and embryonic stem (ES) cells. The *Cmah* targeting vector was assembled from a 129/Sv genomic clone containing exons 4 and 5 of this gene and a neomycin resistance gene driven by the phosphoglycerate kinase 1 promoter (PGK-neoR) as well as a diphtheria toxin A gene fragment driven by the MC1 promoter (DT-A) as positive and negative selection markers, respectively. The construct was created by inserting the PGK-neoR cassette into the NspV site of exon 5 of the *Cmah* gene. The DT-A cassette was then ligated adjacent to the 3′ terminus of the construct.

Generation of mutant mice. Gene targeting and generation of mutant mice were performed essentially as described previously (23). In brief, E14 cells were electroporated with a Bio-Rad Gene Pulser (0.8 kV; 3 μF) using 30 μg of NotI-linearized targeting vector. The electroporated cells were selected in medium containing G418 (125 μg/ml) and screened for homologous recombination by Southern blot analysis of genomic DNA digested with BglI, using both radiolabeled 5′ internal and 3′ external probes. The mutant cells were microinjected into 3.5-day-old C57BL/6J blastocysts, and the embryos were transferred into the uteri of pseudopregnant ICR mice. Mice were used for the determination of immunological features after more than seven backcrosses to the C57BL/6J strain. All mice examined in this study were housed in a specific-pathogen-free facility.

Serum isotype-specific antibody measurement. Serum samples from nonimmunized mice at 8 to 12 weeks of age were subjected to isotype-specific ELISAs. Isotype-specific capturing antibodies were coated onto 96-well ELISA plates, and nonspecific binding was blocked with 1% BSA-supplemented PBS. A serially diluted standard MAb of each isotype (Ancell, Bayport, MN) and diluted serum samples were captured on the wells. The captured Abs were detected with alkaline phosphatase-conjugated isotype-specific goat IgG using a 1420 ARVO SXc (Wallac, Turku, Finland) luminometer.

Determination of antibody production in immunized mice. Eight-week-old mice were immunized after preimmune serum was obtained. Freund's complete adjuvant containing 100 μg of dinitrophenyl (DNP)-keyhole limpet hemocyanin (KLH) was used for primary T-dependent immunization by intraperitoneal injection, and a second boost was performed with the antigen in incomplete adjuvant. For T-independent immunization, 10 μg of DNP-Ficoll in PBS was injected. The anti-DNP titer was measured essentially as above, except that DNP-BSA was used for antibody capture, and a mixed pool of DNP-KLH-immunized serum was used as the standard. The value relative to that of the pooled serum was used to normalize the values obtained from different plates.

B-cell proliferation analysis. In 96-well plates, 100-μl aliquots of B cells at 1×10^5 cells/ml were stimulated in RPMI 1640 medium containing the indicated concentrations of stimulation reagents. After 24 h of incubation, bromodeoxyuridine (BrdU) was added, and the incubation was continued overnight. Incorporated BrdU was detected using a chemiluminescent ELISA system (Roche Diagnostic GmbH) with an 1420 ARVO SXc luminometer.

Immunoblotting and immunoprecipitation of CD22. Splenic B cells were adjusted to 5×10^5 cells/50 μl in RPMI 1640 medium. After preincubation at 37°C, the B cells were stimulated with $F(ab')_2$ anti-mouse IgM (10 μg per 5×10^5 cells) at 37°C. To detect the pattern of tyrosine phosphorylation, cells were lysed in sodium dodecyl sulfate-polyacrylamide gel electrophoresis sample buffer (50 mM Tris-HCl [pH 7.6], 2% sodium dodecyl sulfate, 0.1% pyronin G, 10% glycerol, 2-mercaptoethanol). For immunoprecipitation studies, the stimulated B cells were lysed in NP-40 lysis buffer (1% Nonidet P-40, 150 mM NaCl, 25 mM HEPES [pH 7.4], 5 mM NaF, 2 mM sodium orthovanadate, protease inhibitor cocktail [Nacalai Tesque]), and CD22 was immunoprecipitated with anti-CD22 (Cy34.1) antibody and protein G-Sepharose beads (Amersham Biosciences). In the CD22 immunoprecipitation studies, after a probing step with PT-66, the membrane was reprobed with anti-CD22 polyclonal antibody.

Experimental animals. The studies presented here were performed in accordance with animal care guidelines and were approved by the animal experimental committee of Kyoto University Graduate School of Biostudies.

Microarray data accession numbers. The GEO platform (GPL3465) and experimental results are registered in the Gene Expression Omnibus database under accession number GSE4407.

RESULTS

Sia involvement in GL7 staining of B-cell lines. During B-cell development in mice, the epitope of the MAb GL7 appears and disappears in multiple maturation steps (5, 18, 32,

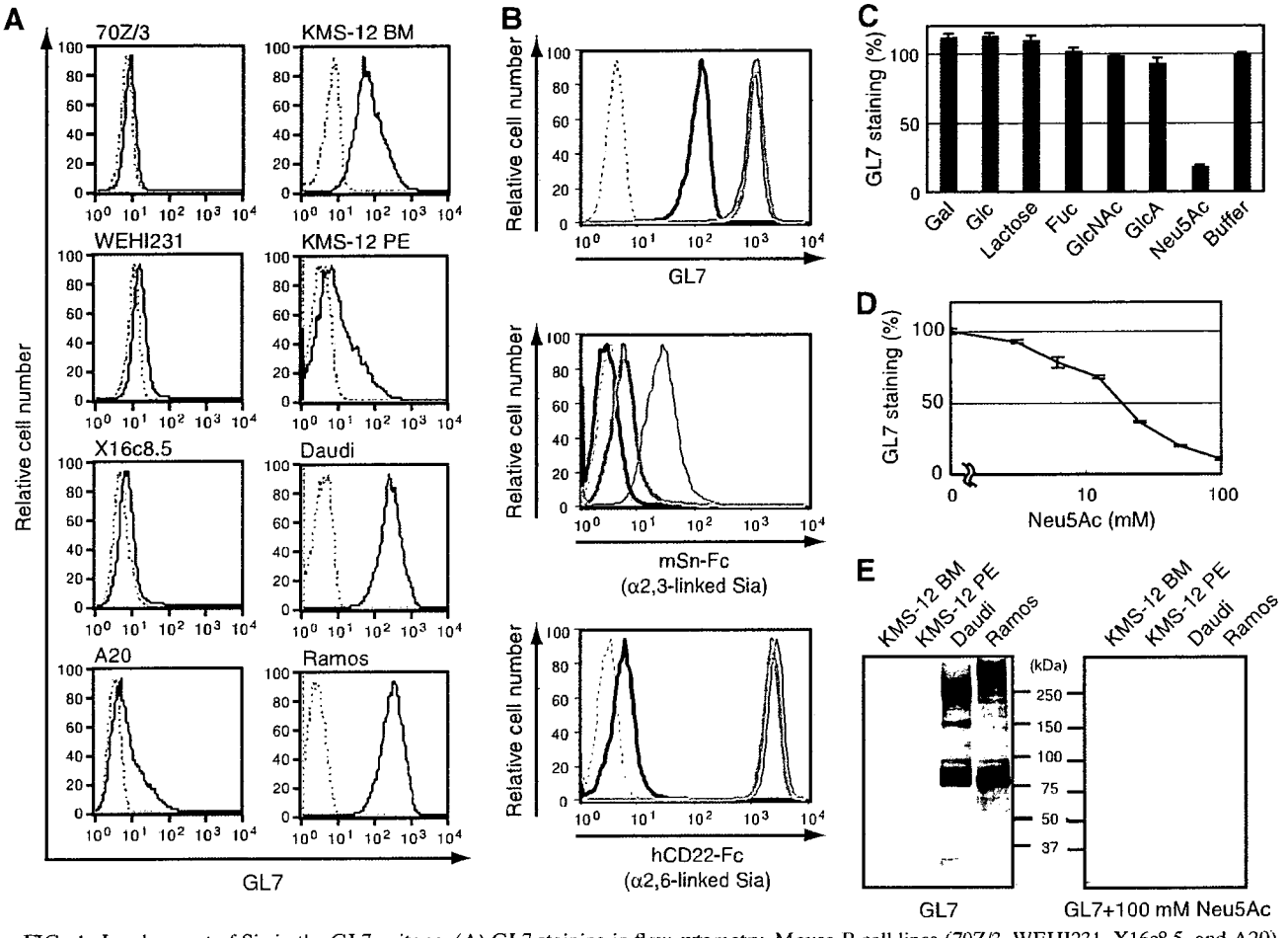

FIG. 1. Involvement of Sia in the GL7 epitope. (A) GL7 staining in flow cytometry. Mouse B-cell lines (70Z/3, WEHI231, X16c8.5, and A20) and human B-cell lines (KMS-12 BM, KMS-12 PE, Daudi, and Ramos) were stained with FITC-conjugated GL7. Black solid lines indicate staining with GL7, and gray dashed lines indicate nonstaining controls. (B) The effect of sialidase treatment on GL7 staining. Daudi cells were treated with sialidase before staining with FITC-conjugated GL7, mSn-Fc, or hCD22-Fc. Gray dashed lines indicate negative controls (nonstaining for GL7 and R-PE-conjugated anti-human IgG for the others), and black thin lines indicate the results without sialidase treatment. Black bold lines indicate the results with *A. ureafaciens* sialidase treatment, and gray bold lines indicate results with *S. enterica* serovar Typhimurium sialidase treatment. Sialidase from *A. ureafaciens* releases α2-3,6,8-linked Sia, whereas sialidase from *S. enterica* serovar Typhimurium is specific to the α2-3 linkage. To confirm the effect of sialidase treatment, changes in cell surface expression of α2,3-linked Sia and α2,6-linked Sia were detected with mSn-Fc and hCD22-Fc chimeric probes precomplexed with R-PE-conjugated anti-human IgG, respectively. (C and D) Effect of free sugars on GL7 binding. Daudi cells were stained with FITC-conjugated GL7 in the presence of 50 mM free sugars (C) or the indicated concentrations of Neu5Ac (D). The data are shown as the relative MFI of each staining. Gal, galactose; Glc, glucose; Fuc, fucose; GlcNAc, *N*-acetylglucosamine; GlcA, glucuronic acid. (E) GL7 blotting of human B-cell lines. Membrane fractions of human B-cell lines (KMS-12 BM, KMS-12 PE, Daudi, and Ramos) were analyzed by GL7 immunoblotting. The addition of 100 mM Neu5Ac during incubation with GL7 reduced most of the staining on blotted membranes.

38). We were interested in the change of GL7 epitope expression, and thus we first assessed the reactivity of this antibody with various B-cell lines, including human germinal center-like Burkitt lymphomas. GL7 showed stronger reactivity toward human B-cell lines than toward mouse B-cell lines (Fig. 1A). The GL7 epitope has been shown to be sensitive to sialidase treatment, although the type of sialidase used in the study reporting this finding was not specified (19). To understand the relationship of GL7 epitopes present on human B-cell lines and mouse activated B cells, we further characterized the determinant on human B-cell lines. The GL7 epitope on Daudi cells was similar to that on mouse activated B cells, as GL7 staining of Daudi cells was also inhibited by sialidase treatment when a broad-range sialidase, *A. ureafaciens* sialidase, was used (Fig. 1B). In contrast, *S. enterica* serovar Typhimurium sialidase, which is specific to α2,3-linked Sia, had no effect (Fig. 1B). To assess the role of Sia and other sugars in GL7 reactivity, we analyzed the inhibitory effects of sugar on GL7 binding. The results clearly showed specificity of Neu5Ac for inhibition (Fig. 1C), and the inhibition was dependent on the Neu5Ac concentration (Fig. 1D). Neu5Ac is a major form of Sia in human cells. GL7 binding was decreased with a metabolic N-glycosylation inhibitor, tunicamycin (see Fig. S1 in the supplemental material). Multiple bands were detected in immunoblotting experiments using the membrane fraction of Daudi cells (Fig. 1E). Thus, it is likely that GL7 recognizes some glycan epitopes, including Sia, rather than some specific protein(s).

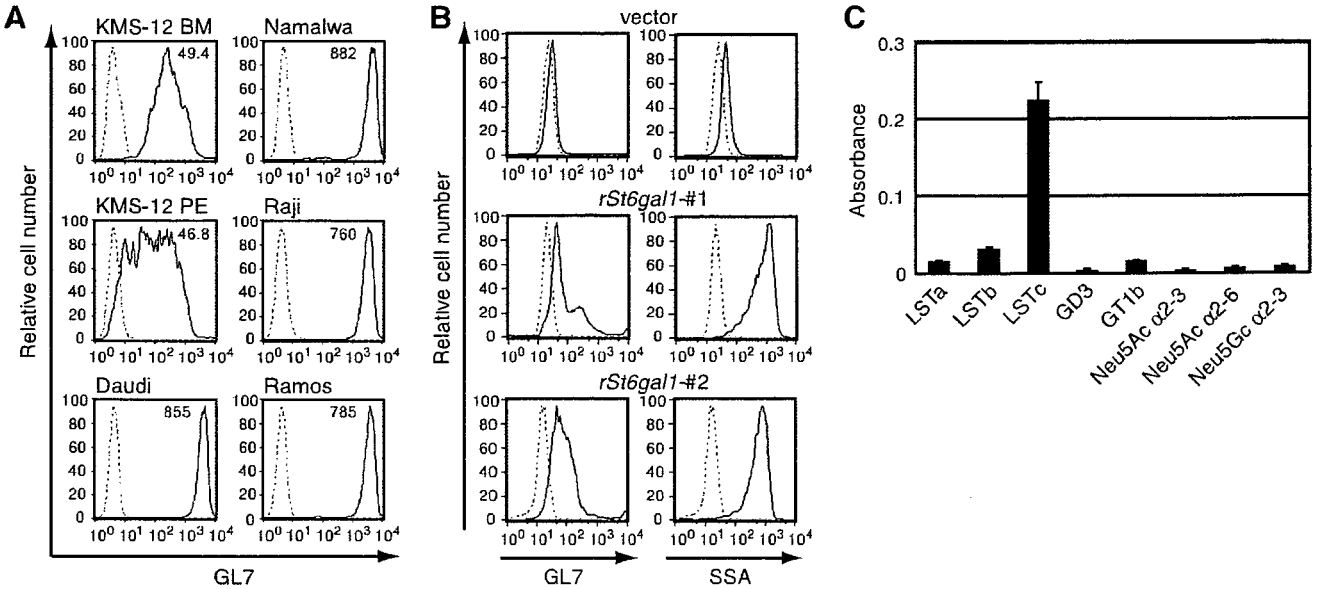

FIG. 2. Involvement of α2,6-linked Neu5Ac in the GL7 epitope. (A) Numerical comparison of GL7 staining among human B-cell lines. The results of GL7 staining of human B-cell lines were numerically compared using MFI values in flow cytometry. To normalize the binding in different cells, the endogenous fluorescence of sample cells (gray dashed lines) was adjusted to an MFI of around 5. For comparison with the gene expression profile, GL7-stained MFI values were divided by the background value. The relative values indicated on the top of each staining were used as the GL7 determinant expression profile. (B) Appearance of the GL7 determinant by ST6GAL1 expression. CHO-K1 clones stably transfected with rat *St6gal1* or an empty vector (as a control) were stained with FITC-conjugated GL7 or FITC-conjugated SSA. The results from two such clones are shown. (C) Carbohydrate binding assay of GL7. Carbohydrate binding was measured using ELISA. Data are shown as the means of triplicate samples, and the bars represent standard errors of the mean. LSTa, Neu5Acα2-3Galβ1-3GlcNAcβ1-3Galβ1-4Glc; LSTb, Galβ1-3(Neu5Acα2-6)GlcNAcβ1-3Galβ1-4Glc; LSTc, Neu5Acα2-6Galβ1-4GlcNAcβ1-3Galβ1-4Glc; GD3, Neu5Acα2-8Neu5Acα2-3Galβ1-4Glc; GT1b, Neu5Acα2-3Galβ1-3GalNAcβ1-4(Neu5Acα2-8Neu5Acα2-3)Galβ1-4Glc; Neu5Ac α2-3, Neu5Acα2-3Galβ1-4Glc; Neu5Ac α2-6, Neu5Acα2-6Galβ1-4Glc; Neu5Gc α2-3, Neu5Gcα2-3Galβ1-4Glc.

Strong correlation between expression of the GL7 epitope and expression of the *ST6GAL1* gene in human B-cell lines. Sia clearly plays an important role in GL7 epitope expression. Interestingly, the GL7 staining of a panel of human B-cell lines was not uniform but, instead, exhibited different intensities (Fig. 1A). Given that a number of bands were detected in immunoblotting experiments, the differences in GL7 epitope expression seemed to be caused by differences in the expression level of an enzyme(s) involved in the biosynthesis of the GL7 epitope glycan rather than differences in carrier protein expression. Therefore, we analyzed the correlation of GL7 epitope expression with the relative level of Sia-related gene expression. The reason to expect such a correlation was that glycosyltransferase activity tends to be regulated through the control of gene expression and substrate accessibility rather than through posttranslational modifications. Six human B-cell lines were stained with GL7 (Fig. 2A), and the relative MFI from flow cytometry was compared with the gene expression profile of the same set of B-cell lines obtained from a newly developed cDNA microarray that can be used to analyze the expression of glycan-related genes. To perform cross-sample comparisons of gene expression among cell lines, we compared poly(A)$^+$ RNA from each B-cell line and commercially available universal reference RNA. The relative gene expression was obtained by dividing the cDNA microarray fluorescence signal from cellular RNA by that of the universal reference (see Table S1 in the supplemental material). From among the genes spotted on the microarray, various genes for sialyltransferases and Sia-metabolizing enzymes were picked to examine their possible relationships to the degree of GL7 staining, because it has been shown that sialyltransferase gene expression might correlate with the surface phenotype of lectin binding (2). We calculated the Pearson's correlation coefficient. Among the sialyltransferase and other Sia-metabolizing enzyme genes, *ST6GAL1* showed the strongest correlation between its expression profile and the GL7 staining profile (Table 1). This result indicates that *ST6GAL1* expression could be responsible for the biosynthesis of the GL7 epitope in these human B-cell lines. ST6GAL1 transfers Sia onto a Gal residue of terminal *N*-acetyllactosamine (LacNAc; Gal β1-4GlcNAc) with an α2,6 linkage (42), and B cells have been shown to express this enzyme (20, 64). This indicates that the terminal transferase reaction by ST6GAL1, but not the supply of the substrate, is the rate-limiting step in GL7 epitope biosynthesis in these cells. Interestingly, a negative correlation was found between GL7 staining and the expression of *SIAE*, a gene encoding Sia 9-*O*-acetylesterase (Table 1). Although Sia 9-*O*-acetylesterase cleaves the *O*-acetyl group of Sia, *SIAE* is expressed in cell types expressing its substrate, 9-O-acetylated Sia (57). If the degree of 9-O acetylation were to correspond with the level of *SIAE* expression, GL7 binding might be negatively affected by 9-*O*-acetyl modification, similar to CD22 (56).

Effect of ST6GAL1 overexpression on GL7 epitope expression. Data from the correlation index calculation suggest that GL7 recognizes α2,6-linked Sia on N-glycan and that the expression of the GL7 epitope on human B cells depends mainly

TABLE 1. Pearson's correlation index analysis of Sia-related genes[a]

Index	*P* value	Gene name	Encoded enzyme
0.937	5.87E-3	*ST6GAL1*	ST6Gal I
0.806	5.30E-2	*ST3GAL3*	ST3Gal III
0.551	2.57E-1	*CMAH*	Pseudogene for CMP-Neu5Ac hydroxylase
0.473	3.44E-1	*ST3GAL2*	ST3Gal II
0.215	6.82E-1	*SLC35A1*	CMP-Sia transporter
0.173	7.43E-1	*ST8SIA1*	ST8Sia I
0.142	7.89E-1	*ST3GAL6*	ST3Gal VI
0.137	7.96E-1	*PGM3*	GlcNAc-6-P mutase
0.096	8.56E-1	*GMPPB*	GDP-Man pyrophosphorylase
0.052	9.22E-1	*ST6GALNAC2*	ST6GalNAc II
−0.103	8.47E-1	*ST8SIA3*	ST8Sia III
−0.196	7.10E-1	*ST8SIA4*	ST8Sia IV/PST
−0.210	6.89E-1	*GNE*	UDP-GlcNAc-2-epimerase/ ManNAc kinase
−0.283	5.87E-1	*ST6GALNAC6*	ST6GalNAc VI
−0.442	3.80E-1	*ST3GAL5*	ST3Gal V
−0.448	3.72E-1	*ST6GALNAC1*	ST6GalNAc I
−0.452	3.68E-1	*ST8SIA5*	ST8Sia V
−0.508	3.04E-1	*SAS*	Neu5Ac-9-P synthase
−0.639	1.72E-1	*ST6GALNAC4*	ST6GalNAc IV
−0.678	1.39E-1	*NEU3*	Membrane sialidase
−0.696	1.25E-1	*NEU1*	Lysosomal sialidase
−0.739	9.30E-2	*ST8SIA2*	ST8Sia II/STX
−0.742	9.12E-2	*ST3GAL4*	ST3Gal IV
−0.898	1.52E-2	*ST3GAL1*	ST3Gal I
−0.938	5.62E-3	*SIAE*	Sia-9-*O*-acetylesterase

[a] Pearson's correlation coefficient (index) values of relative gene expression in the microarray against relative GL7 staining MFI among six B-cell lines were calculated for sialyltransferase genes and Sia metabolism-related genes. A positive value indicates the presence of a correlation between gene expression and staining. A negative value indicates the presence of a negative correlation. Index values are also expressed as *P* values.

on *ST6GAL1* expression. To evaluate these findings, we explored the ST6GAL1 expression dependence of GL7 epitope expression. CHO-K1 cells are known to lack α2,6-linked Sia on their cell surfaces. As expected, the parental CHO-K1 cells were GL7 negative (data not shown), as were vector-transfected CHO-K1 cells (Fig. 2B). In contrast, rat *ST6GAL1* (r*St6gal1*)-transfected CHO-K1 cells showed a marked increase in GL7 staining (Fig. 2B). The increase in GL7 staining upon r*St6gal1* expression coincided with the increase in staining by SSA, a plant lectin which reacts with Sia α2,6-Gal/GalNAc on glycans. As CHO-K1 cells are nonimmune cells, GL7 seemed to recognize α2,6-linked Neu5Ac-containing sugar chains on various proteins. Immunoblotting analysis of these stable clones further clarified that the introduction of r*St6gal1* was sufficient to give rise to bands on the blot. The membrane fractions of both CHO-K1 stable clones and human B-cell lines resulted in multiple bands (data not shown).

Glycan-binding assay of GL7. To confirm that GL7 is an antiglycan antibody that recognizes α2,6-linked Sia and also to determine the fine specificity of the epitope, we examined GL7 binding to various glycan probes (65) by ELISA. GL7 bound to LSTc (Neu5Acα2-6Galβ1-4GlcNAcβ1-3Galβ1-4Glc) but not to its structural isomer with α2–3 linked Neu5Ac, LSTa (Neu5Acα2-3Galβ1-3GlcNAcβ1-3Galβ1-4Glc) (Fig. 2C). Interestingly, GL7 did not bind to Neu5Acα2-6Galβ1-4Glc (sialyllactose) in spite of the existence of α2,6-linked Neu5Ac in the probe. The glucose (Glc) of the reducing terminal was destroyed during probe preparation for coupling with streptavidin. Thus, it is likely that the structure of Neu5Acα2-6Gal is not sufficient for GL7 binding but that the binding requires at least a trisaccharide for optimal recognition or GlcNAc in the underlying lactosamine. Taking all of the results into consideration, we concluded that GL7 recognizes α2,6-linked Sia-containing glycan chains that are often found on N-glycans of various proteins.

A shift in the major Sia species, Neu5Gc to Neu5Ac, in the mouse germinal center reaction. It was still not clear why GL7 failed to react with mouse mature B cells, given that these cells abundantly express α2,6-linked sialoglycans, as St6gal1 is also expressed in these cells (20, 64). The dominant difference in sialylation between mice and humans occurs in the Sia modification at the C-5 position (60). Humans predominantly express Neu5Ac, whereas the major Sia in mice is Neu5Gc (Fig. 3A). It is possible that the change in GL7 reactivity could be a consequence of the change in sia modification. Neu5Gc modification in biosynthesis is regulated by the Cmah reaction in the cytosol, which metabolically gives rise to the donor, CMP-Neu5Gc, for a subsequent sialyltransferase reaction(s) in the Golgi apparatus (Fig. 3B) (24, 25). We therefore asked whether mouse B cells undergo a change in Sia species, from Neu5Gc to Neu5Ac, in GL7-positive cells. We first stained the germinal centers with GL7 and the lectin domain of mouse CD22 (mCD22-Fc), because mouse CD22 demonstrates a marked preference for Neu5Gc-bearing over Neu5Ac-bearing α2,6-linked sialoglycan ligands (26, 44, 50). As shown in Fig. 3C, in the SRBC-immunized mouse spleen, GL7-positive germinal centers were specifically excluded by mCD22-Fc recognition. This complementarity of staining appeared to be the result of the probe preferences, Neu5Ac for GL7 and Neu5Gc for mCD22-Fc, respectively. We then assessed Cmah expression and the Neu5Ac-Neu5Gc ratio in GL7-positive germinal center B cells. Germinal center (GL7-bound) cells showed severely reduced expression of Cmah, and this reduction coincided with the loss of Neu5Gc in the membrane fraction of the cells (Fig. 3D). In contrast, GL7-negative SRBC-immunized B cells were not significantly different from nonimmunized splenic B cells. Thus, the gain of GL7 staining reflected the loss of the CD22 ligand in germinal center B cells due to the repression of Cmah.

Real-time PCR analysis during mouse B cell activation. LPS stimulation induces the GL7 epitope in B cells (28). Therefore, we adopted this system to assess the enzyme (gene) responsible for GL7 epitope expression. Cmah is responsible for Sia species change, and St6Gal1 is responsible for Sia linkage biosynthesis. We examined the expression of *Cmah* and *St6gal1* to determine whether changes in the expression of these genes could account for the GL7 epitope induction detected in B-cell activation events. In real-time RT-PCR experiments, *Cmah* expression showed an 80% reduction in LPS-stimulated B cells compared with unstimulated splenic B cells after 48 h of incubation (Fig. 4A). This reduction was already detectable after 3 h of culture. Despite the slightly enhanced expression level of α2,6-linked Sia-containing glycan probed with SSA, *St6gal1* expression showed a subtle reduction in activated B cells after 48 h (Fig. 4A and B). *Cmah* reduction appears to play a prominent role in the appearance of the GL7 epitope in activated B cells. Retrovirus-mediated ectopic *Cmah* expression consistently reduced the expression of the GL7 epitope in